Neuron

Article

Encoding of 3D Head Orienting Movements in the Primary Visual Cortex

Graphical Abstract

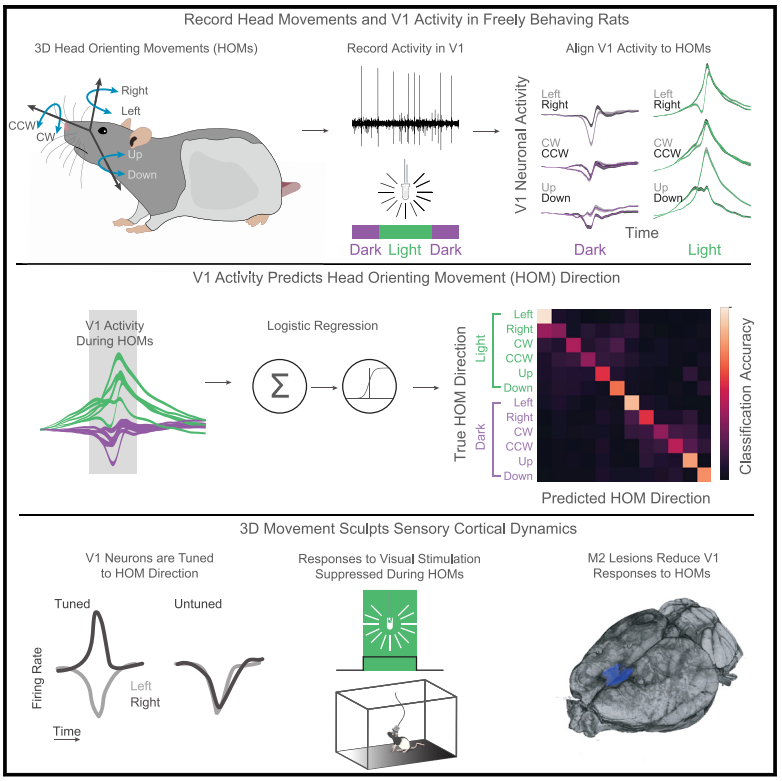

Highlights

- Primary visual cortex (V1) encodes 3D head-orienting movements (HOMs)
- V1 neurons are modulated by HOMs depending on light and are tuned to HOM direction
- Responses to visual stimulation are suppressed during HOMs
- HOM encoding depends on secondary motor cortex (M2)

Authors

Grigori Guitchounts, Javier Masís, Steffen B.E. Wolff, David Cox

Correspondence

guitchounts@fas.harvard.edu

In Brief

Guitchounts et al. find that the primary visual cortex (V1) of freely moving rats encodes 3D orienting movements of the head (HOMs). V1 is suppressed or enhanced by HOMs, depending on lighting condition, and individual neurons encode HOM direction. This encoding depends on secondary motor cortex (M2).

Guitchounts et al., 2020, Neuron *108*, 1–14
November 11, 2020
https://doi.org/10.1016/j.neuron.2020.07.014

CellPress

Please cite this article in press as: Guitchounts et al., Encoding of 3D Head Orienting Movements in the Primary Visual Cortex, Neuron (2020), https://doi.org/10.1016/j.neuron.2020.07.014

Neuron

CellPress

Article

Encoding of 3D Head Orienting Movements in the Primary Visual Cortex

Grigori Guitchounts,[1,2,3,6,*] Javier Masís,[1,2] Steffen B.E. Wolff,[1,4] and David Cox[1,2,5]
[1]Center for Brain Science, Harvard University, Cambridge, MA 02138, USA
[2]Department of Molecular and Cellular Biology, Harvard University, Cambridge, MA 02138, USA
[3]Program in Neuroscience, Harvard University, Boston, MA 02115, USA
[4]Department of Organismic and Evolutionary Biology, Harvard University, Cambridge, MA 02138, USA
[5]IBM Research AI, Cambridge Research Center, Cambridge, MA 02142, USA
[6]Lead Contact
*Correspondence: guitchounts@fas.harvard.edu
https://doi.org/10.1016/j.neuron.2020.07.014

SUMMARY

Animals actively sample the sensory world by generating complex patterns of movement that evolve in three dimensions. Whether or how such movements affect neuronal activity in sensory cortical areas remains largely unknown, because most experiments exploring movement-related modulation have been performed in head-fixed animals. Here, we show that 3D head-orienting movements (HOMs) modulate primary visual cortex (V1) activity in a direction-specific manner that also depends on light. We identify two overlapping populations of movement-direction-tuned neurons that support this modulation, one of which is direction tuned in the dark and the other in the light. Although overall movement enhanced V1 responses to visual stimulation, HOMs suppressed responses. We demonstrate that V1 receives a motor efference copy related to orientation from secondary motor cortex, which is involved in controlling HOMs. These results support predictive coding theories of brain function and reveal a pervasive role of 3D movement in shaping sensory cortical dynamics.

INTRODUCTION

Animals sample the visual world by producing complex patterns of movements (Yarbus, 1967). Primates, birds, cats, fish, and insects move their eyes, heads, or bodies to stabilize the gaze, shift gaze, sample the visual scene, or estimate distance using parallax motion cues (Kral, 2003; Ellard et al., 1984; Land, 1999, 2015; Binda and Morrone, 2018). Saccadic eye movements in primates are accompanied by a suppression of neural activity in visual areas, which serves to reduce blur during fast movement and produce an active sampling of the scene (Binda and Morrone, 2018; Krock and Moore, 2014; Mohler and Cechner, 1975; Thilo et al., 2004; Niemeyer and Paradiso, 2018; Sylvester et al., 2005; McFarland et al., 2015; Thiele et al., 2002; Wurtz and Sommer, 2004). Freely moving rodents also make complex patterns of head and eye movements (Hoy et al., 2016; Wiltschko et al., 2015; Wallace et al., 2013; Meister and Cox, 2013; Meyer et al., 2018; Land, 1999, 2015). For example, rodents use head movements to estimate distances when jumping across a gap (Legg and Lambert, 1990; Ellard et al., 1984), and rats move their eyes to stabilize their gaze (Wallace et al., 2013; Meister and Cox, 2013). Similarly, mice also move their eyes under head-fixed conditions (Sakatani and Isa, 2007; Itokazu et al., 2018). However, the neural consequences of many of these movements remain unclear.

Despite the number of various movements animals make to support visual perception, vision has typically been studied by presenting stimuli to restrained animals. In this framework, vision is a passive sense and visual processing is a feedforward computation in which information enters the brain through the retina and is processed one stage at a time as it travels deeper into the brain, through thalamus and cortex (Hubel and Wiesel, 1962; Felleman and Van Essen, 1991; DiCarlo and Cox, 2007; Miller, 2016). Consistent with this view, the majority of neurophysiological experiments on primary sensory cortical areas have found that information in those areas is chiefly sensory in nature.

Importantly, visual cortical areas receive a multitude of feedback and modulatory inputs that influence sensory processing; this feedback may afford visual areas with information required to distinguish between self-generated sensory signals and those that arise in the outside world (Schneider et al., 2014; Cullen, 2019; Crapse and Sommer, 2008). One candidate origin for efference copy signals in visual cortex is secondary motor cortex (M2), a medial prefrontal structure linking multiple motor and sensory regions (Barthas and Kwan, 2017). Anatomical evidence has suggested that M2 is a motor associational region because it projects both to subcortical targets, such as superior colliculus (Leonard, 1969; Barthas and Kwan, 2017; Zhang et al., 2016), brainstem nuclei controlling eye movements (Leichnetz et al.,

Please cite this article in press as: Guitchounts et al., Encoding of 3D Head Orienting Movements in the Primary Visual Cortex, Neuron (2020), https://doi.org/10.1016/j.neuron.2020.07.014

1987; Stuesse and Newman, 1990), and the spinal cord (Gabbott et al., 2005; Donoghue and Wise, 1982; Barthas and Kwan, 2017), as well as multimodal cortical areas, such as primary sensory, retrosplenial, and posterior parietal cortices (Barthas and Kwan, 2017). Furthermore, M2 has extensive bidirectional connections with visual cortex (Zingg et al., 2014; Zhang et al., 2016; Barthas and Kwan, 2017). Functional evidence further supports the idea of M2's involvement in orienting movements. Electrical stimulation of M2 results in eye and orienting movements (Sinnamon and Galer, 1984; Hall and Lindholm, 1974; Itokazu et al., 2018), usually contralateral to the stimulated hemisphere, and optogenetic stimulation of M2 axons over V1 leads to turning behavior in head-fixed mice (Leinweber et al., 2017). Conversely, temporary unilateral inactivation of M2 leads to contralateral neglect in a memory-guided orienting task (Erlich et al., 2011), and unilateral lesions of M2 result in hemilateral neglect (Barth et al., 1982). Neuronal activity correlates of orienting movements have also been recorded in M2, both in the context of behavioral tasks (Erlich et al., 2011; Itokazu et al., 2018) and in freely orienting animals (Kanki et al., 1983; Mimica et al., 2018). These anatomical, physiological, and functional lines of evidence implicate M2 as a potential source of movement-related signals in V1, which may be used to process self-generated sensory signals.

One defined means through which sensory cortices encode movement signals is via a unidimensional state variable that corresponds to the animal's overall locomotion. Such movement-related signals have been found in a myriad of sensory brain regions (Niell and Stryker, 2010; Fu et al., 2014; Polack et al., 2013; Saleem et al., 2013; Keller et al., 2012; Schneider et al., 2014; Roth et al., 2016; Williamson et al., 2015; Erisken et al., 2014; Clancy et al., 2019; Meyer et al., 2018; Leinweber et al., 2017; Vélez-Fort et al., 2018; Stringer et al., 2019; Musall et al., 2019). This locomotion signal can have varied effects on sensory cortices. For example, although movement suppresses activity in mouse auditory cortex (Schneider et al., 2014), during locomotion on a treadmill, cells in primary visual cortex (V1) increase their activity, reflect running speed, and increase the gain on encoding of visual stimuli (Niell and Stryker, 2010; Fu et al., 2014; Polack et al., 2013; Saleem et al., 2013; Keller et al., 2012).

In addition to locomotion per se influencing neural activity, specific movements have been shown to modulate sensory cortical activity, including orofacial movements and movements associated with different directions of visual flow (Leinweber et al., 2017; Vélez-Fort et al., 2018; Stringer et al., 2019; Musall et al., 2019). However, such studies have primarily been performed in head-fixed rodents, which has made it difficult to answer whether sensory areas are modulated by naturalistic self-generated movements that support sensory sampling. Here, by recording activity in V1 during free behavior in rats, we demonstrate that head-orienting movements are associated with suppression or enhancement of neural activity in visual cortical neurons in the dark or light, respectively. Furthermore, V1 activity reflected the direction of head movement, both in the dark and in the light, with individual neurons tuned independently either in the dark or light. Responses to visual stimulation were modulated bidirectionally during movement, with responses enhanced or suppressed during overall movement or orienting movements of the head, respectively, relative to rest. Finally, V1 responses to orienting movements and direction encoding depended on M2. Our results demonstrate that cortical sensory dynamics encode the direction of self-generated movements in 3D, provide evidence for direction-specific efference copy signaling in V1, and raise the possibility that head-orienting movements in rodents serve the same functional purpose as saccades do in primates (Morris and Krekelberg, 2019).

RESULTS

To investigate the impact of spontaneous movements on sensory cortical dynamics, we recorded neuronal activity using tetrode arrays targeting layer 2/3 of rat V1 while the animals behaved freely in a home-cage arena (Figures 1A, 1B, S1A, and S2A–S2E). Movements were captured using a head-mounted inertial measurement unit (IMU) (see Method Details). Recordings were made continuously (24/7) and split into 2-h sessions in the dark or light in order to investigate the effects of movement in the absence or presence of visual cues, respectively. The timing of lighting conditions was pseudo-randomized to offset possible circadian effects on V1 activity (Figures S1A and S1B).

We focused our analysis on 3D orienting movements of the head, which we refer to as head-orienting movements (HOMs), as well as total acceleration, which we term overall movement. Bouts of overall movement rarely also contained HOMs (~8% of the time). This dissociation enabled us to distinguish overall-movement-related activity—such as forward locomotion—from activity related to particular directions of orienting head movements (Figures 1C and 1D).

Animals spent <3% of time above the velocity threshold of 100°/s (Figures 1E and 1F). The rate of HOMs was somewhat higher at the beginning of each session but relatively steady throughout (Figures S1C and S1D). We focused our analysis on HOMs along individual directions, although about 25% of the time, animals made movements along multiple axes (Figure S1E). Individual animals made similar numbers of opposing turns (Figures S1F and S1G), and across rats, above-threshold velocities in opposing directions (e.g., left versus right) could not be distinguished from one another (Figure 1G). Thus, although the animals moved more in the dark, the head-velocity dynamics were similar between the two lighting conditions, which allowed us next to ask how V1 dynamics are affected by general movements or HOMs in the dark or light.

V1 Activity Is Enhanced by Overall Movement

As previously observed in V1 of head-fixed mice running on spherical treadmills, multiunit activity (MUA) firing rates were indeed higher during overall movement compared to rest, both in the dark and the light (Figures 2A–2C). To examine the cellular basis for movement modulation of V1, we sorted the extracted multiunit spikes into single units (Figures S2F–S2J). Sorted single units were classified into regular-spiking putative excitatory units (RSUs) and fast-spiking putative inhibitory units (FSUs) based on waveform shape.

Firing rates of single units were on average higher during epochs of overall movement compared to rest in the dark and

Please cite this article in press as: Guitchounts et al., Encoding of 3D Head Orienting Movements in the Primary Visual Cortex, Neuron (2020), https://doi.org/10.1016/j.neuron.2020.07.014

CellPress

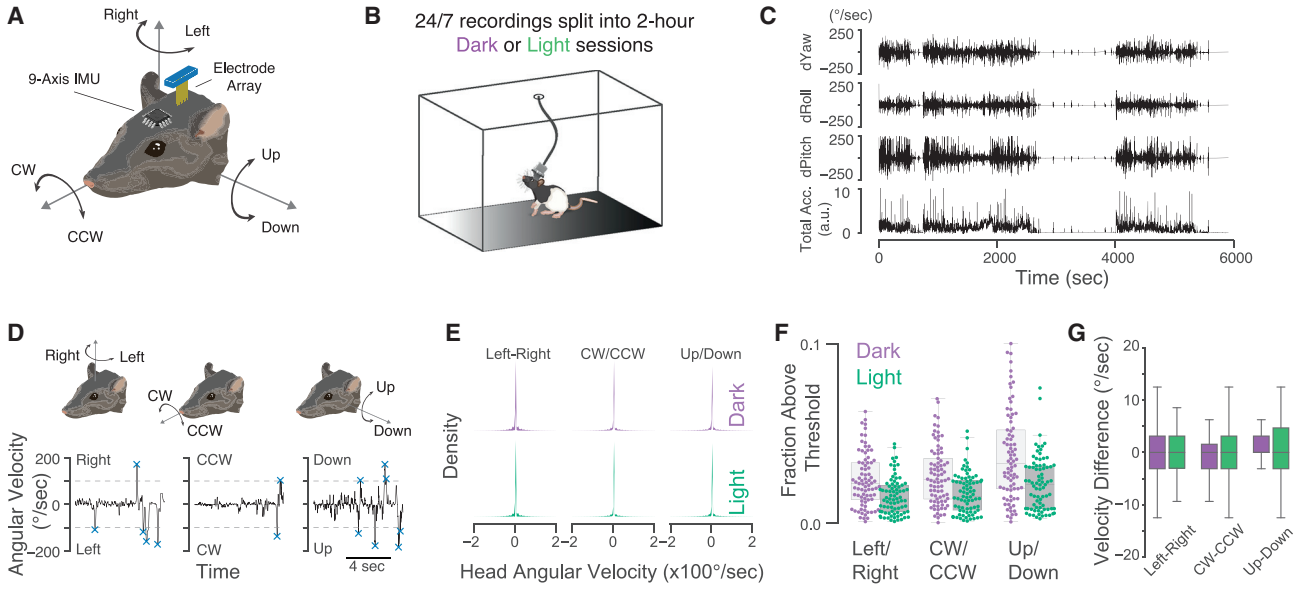

Figure 1. Freely Moving Rats Make 3D Head-Orienting Movements (HOMs) in Dark or Light

(A) Angular velocity of the head was measured using a head-mounted sensor, and neural activity in V1 was measured using chronically implanted electrode arrays.

(B) During the 24/7 recordings, rats were free to explore in their home cage either in the light or in the dark, with ~12 h per lighting epoch. Each epoch was then split into 2-h sessions for analysis.

(C) Example traces from one session showing angular velocity, derivatives of the yaw, roll, and pitch angles of the head, as well as the overall movement (total acceleration).

(D) HOMs were extracted by finding peaks of the angular velocity signals that crossed a threshold (100°/s).

(E) Mean distributions of the head angular velocities along the left-right, CW-CCW, and up-down axes in the dark (top) and light (bottom) from n = 81 sessions in the dark and n = 79 sessions in the light. Shading represents 2 × SD across sessions.

(F) Animals spent 2.92% ± 0.12% of the time above the angular velocity threshold in the dark and 1.78% ± 0.08% in the light (Mann-Whitney U test: $p = 8 \times 10^{-12}$). Each dot is one session.

(G) Differences in median above-threshold velocities across sessions and rats for opposing HOM directions were centered around zero (Wilcoxon test of left-right velocity differences p = 0.59 in dark and p = 0.67 in light; CW-CCW p = 0.51 in dark and p = 0.92 in light; and up-down p = 0.0042 in dark and p = 0.13 in light). See also Figure S1.

the light, with RSU rates affected more than FSUs (Figure 2D). Approximately a fifth of individual RSUs had significantly modulated firing rates during movement, with the vast majority of the significantly modulated firing rates increasing during movement. A smaller fraction of FSUs had significantly modulated firing rates during movement, and these were more bidirectionally modulated than RSUs (Figure 2E). RSU mean firing rates were more strongly modulated by the animals' overall movement than the lighting condition (Figure 2D), further highlighting the significance of movement on neural coding in V1. Approximately 75% of single units were responsive to overall movement onset and offset (Figure 2F), in contrast to the small fraction of units whose mean firing rates changed during overall movement.

To address the possibility that sleep contributed to lower firing rates during rest bouts, we examined V1 activity as a function of the length of rest or movement bout duration (Figures S2K–S2M). Previous reports of the statistics of rat sleep showed that rats sleep in bouts of ~16–20 min (Hengen et al., 2016; Watson et al., 2016; Timo-Iaria et al., 1970). We thus analyzed firing rates during sub-minute epochs of rest or movement. V1 activity was modulated across a range of these short rest durations, indicating that differential firing rates during rest and movement are likely not due to a confounding factor, such as sleep (Figures S2K–S2M). Thus, as in previous reports in head-fixed (Niell and Stryker, 2010; Polack et al., 2013; Keller et al., 2012; Saleem et al., 2013) or freely moving (Meyer et al., 2018) mice, V1 activity in freely behaving rats was modulated by overall movement.

Bidirectional Responses in the Light and Dark in V1 Encode 3D HOM Direction

In contrast to the increased activity in V1 during overall movement, HOMs were correlated with a sub-second suppression of MUA firing rates in the dark and an increase of firing rates in the light (Figures 3A–3D). These patterns were consistent across animals (Figure S3A). In the light, V1 activity peaked after peak head velocity, at temporal delays roughly corresponding to previously reported response times to visual stimulation in rat V1 (Figure S3B; Tafazoli et al., 2017). Across all HOMs, V1 activity deviated from baseline as early as 920 ms before movement onset (Figure S3B), suggesting that these signals reflect a motor or predictive signal rather than sensory reafference. Finally, the differences in MUA responses to opposing HOM directions

Please cite this article in press as: Guitchounts et al., Encoding of 3D Head Orienting Movements in the Primary Visual Cortex, Neuron (2020), https://doi.org/10.1016/j.neuron.2020.07.014

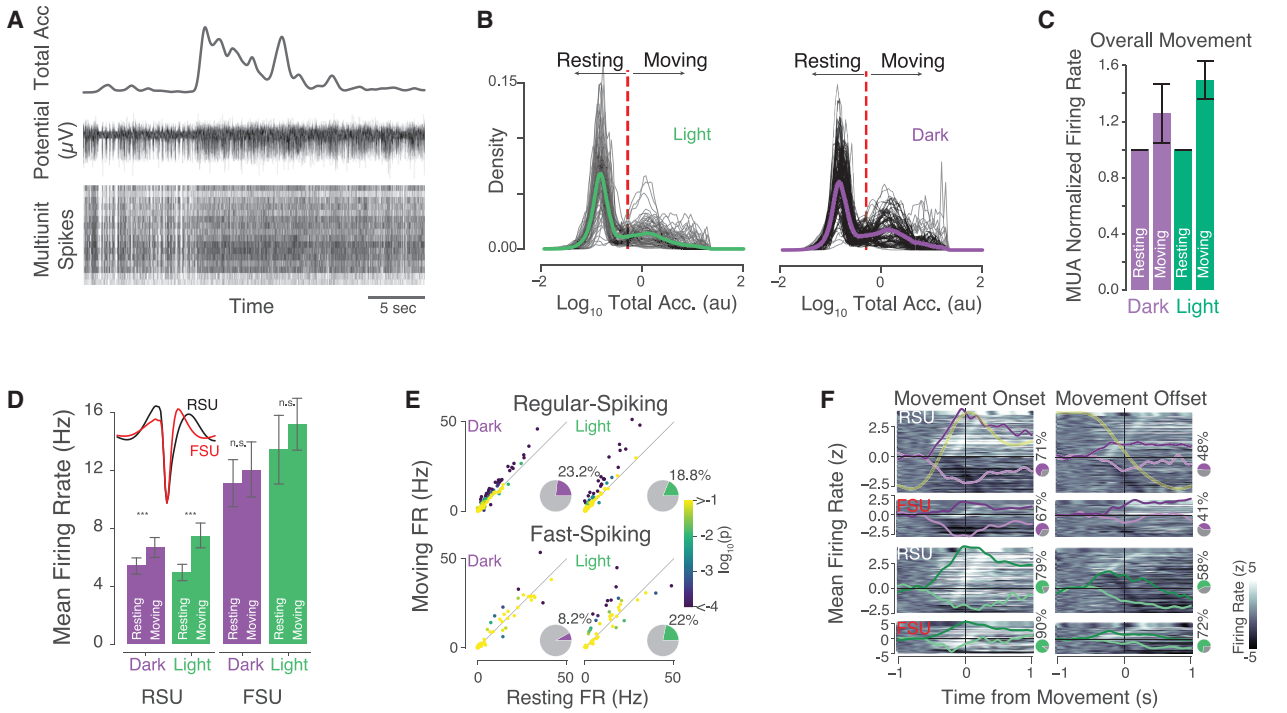

Figure 2. V1 Activity Is Enhanced during Overall Movement

(A) Example bout of movement (top) aligned to a raw bandpass-filtered trace from one electrode (middle) and extracted multi-unit spikes (bottom).

(B) Classification of behavior into resting or moving based on total acceleration. Probability density plots of total acceleration (black, individual sessions; green/purple, mean across sessions) show a bimodal distribution. Dotted red lines show manually selected classification boundary.

(C) Multiunit activity (MUA) firing rates were on average 25.9% and 49.6% higher during overall movement compared to rest in the dark and light, respectively ($p < 1 \times 10^{-10}$ for both, Wilcoxon test; error bars, median absolute deviation).

(D) Mean regular-spiking unit (RSU) (putative excitatory cells) firing rates were higher during overall movement compared to rest in dark ($p = 1.45 \times 10^{-7}$) or light ($p = 5.13 \times 10^{-16}$; Wilcoxon rank-sums tests); mean fast-spiking units (FSUs) (putative inhibitory cells) firing rates were higher than, but not significantly affected by, overall movement (dark, $p = 0.19$; light, $p = 0.046$). Lighting condition did not affect firing rates during overall movement (dark versus light; $p = 0.22$) or rest (dark versus light; $p = 0.16$) in RSUs or during movement (dark versus light; $p = 0.02$) or rest (dark versus light; $p = 0.06$) in FSUs. Inset: mean waveforms of RSUs and FSUs are shown.

(E) Firing rates of individual units during overall movement and rest. Inset pie charts: percentages of units with firing rates modulated by overall movement are shown. 23.2% (33/142) of RSUs and 8.2% (5/61) of FSUs were significantly modulated by overall movement in the dark (permutation test; $p < 0.05$, Bonferroni corrected), although 18.8% (21/112) of RSUs and 22% (11/50) of FSUs were modulated by overall movement in the light. Each dot represents one neuron; color represents p value in permutation test.

(F) Firing rates aligned to overall movement onsets and offsets. Heatmaps showing *Z*-scored firing rates of individual units (y axis) over a 2-s period (x axis) aligned to overall movement onsets (left column) or offsets (right). Lines show the mean overall movement (yellow) and mean *Z*-scored firing rates (purple, dark; green, light); means are separated by sign of activity in the 0.5 s around movement detection (darker traces, positive responses; lighter, negative). Pie charts show percentages of units significantly modulated by overall movement onsets or offsets (permutation test; $p < 0.05$, Bonferroni corrected).

See also Figure S2.

could not be explained by head velocity alone, because the median above-threshold head velocities in opposing directions were similar (Figure 1G).

A large fraction of single units was responsive during HOMs (Figures 3E–3G). The responses of V1 single units during HOMs were heterogeneous in directionality and timing, with the majority of significantly modulated units suppressed in the dark and excited in the light. Although RSUs were equally likely to be suppressed or excited by HOMs in the dark, ~75% of FSUs were suppressed (Figure 3G). Although most cells had maximal responses following peak velocity, ~25%–40% peaked before (Figure 3H), again highlighting the predictive nature of these signals. Finally, V1 responses to HOMs were not sparse: out of 6 examined directions of movement, V1 single units responded significantly to an average of ~4 directions (Figure 3I). Thus, 3D movement in freely moving animals shapes V1 dynamics.

To address whether observed V1 dynamics encode specific movements, we built a logistic regression classifier that took as inputs the session- and tetrode-averaged MUA in the 500 ms around peak head velocity and predicted the HOM direction (Figures 4A and 4B). The models performed well above chance, with decoding performance higher in the light than in the dark. Further, decoding performance increased as a function of the number of sessions used in training (Figure 4C). Performance peaked in the 100 ms after peak velocity and dropped to chance 2 s before or after peak velocity (Figure 4D).

Please cite this article in press as: Guitchounts et al., Encoding of 3D Head Orienting Movements in the Primary Visual Cortex, Neuron (2020), https://doi.org/10.1016/j.neuron.2020.07.014

CellPress

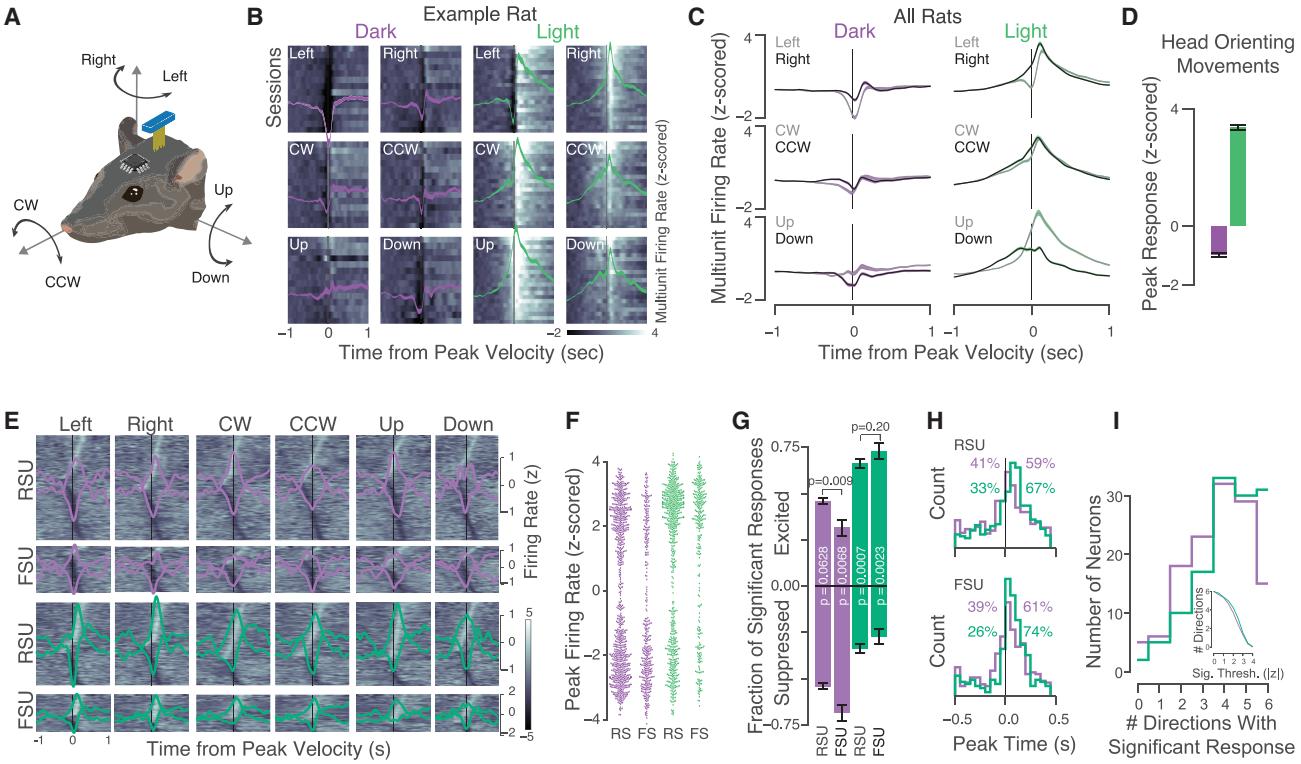

Figure 3. Bidirectional Modulation of V1 Activity during HOMs

(A) Measuring V1 activity during 3D HOMs.

(B) Example of *Z*-scored MUA firing rates from one rat's trial- and tetrode-averaged sessions aligned to extracted left and right (top row), clockwise and counterclockwise (middle row), and up and down (bottom row) HOMs in the dark (purple, first two columns) and light (green, last two columns). Shading in overlaid mean traces represents SEM.

(C) HOM responses averaged across rats, overlaying responses to opposing directions (mean ± SEM).

(D) In contrast to increased mean firing rates aligned to general movement, MUA firing rates were suppressed in the dark and enhanced in the light when aligned to HOMs.

(E) Heatmaps of HOM-aligned responses in RSUs (n = 142 in dark; n = 112 in light) and FSUs (n = 61 in dark; n = 50 in light). Rows represent individual neurons; lines depict means of enhanced and suppressed responses.

(F) Peak responses of single units to HOMs in the ±0.5 s around peak velocity were bimodal (responses pooled across HOM directions).

(G) Of the significantly responding cells (determined by a shuffle test against a baseline window −1 to −0.5 s before peak velocity), half of the RSUs and the majority of FSUs were suppressed in the dark (53.95% ± 1.70% of RSUs and 68.72% ± 4.20% of FSUs), and the majority of both types of units were excited in the light (66.17% ± 2.05% of RSUs and 72.11% ± 3.79% of FSUs; mean ± SEM across HOM directions; p values above bars indicate results of t tests).

(H) Timing of peak firing rates relative to peak velocity of the head. Responses before peak velocity were more common in the dark than in the light for both RSUs ($p = 9 \times 10^{-4}$) and FSUs ($p = 6 \times 10^{-4}$, Fisher's exact test).

(I) V1 single units responded to a mean of 3.70 ± 0.14 HOM directions in the dark and 4.25 ± 0.13 in the light out of the possible 6 directions (mean ± SEM). Inset: number of directions with significant responses as a function of response threshold is shown.

See also Figure S3.

A logistic regression decoder trained to discriminate opposing HOM directions (e.g., left versus right) using single-unit responses performed well above chance (Figures 4E–4I), with performance exceeding chance prior to movement onset (Figure 4F), consistent with the possibility that a significant portion of the responses were orienting based rather than sensory. RSUs and FSUs encoded HOM direction in the dark and light (Figures 4G–4I), with best performance in the light and mixtures of RSUs and FSUs outperforming models that used only one neuron type. Surprisingly, although RSUs encoded HOM direction better than FSUs in the light, their direction encoding in the dark was slightly poorer than FSUs' in the dark (Figures 4G–4I). Thus, V1 single-unit activity reflected not only overall movement signals (Figure 2) but HOM direction as well. These results support the idea that movement direction is encoded in V1, even in the absence of visual input, and that this information is present even before the movements are executed.

V1 Single Units Are Tuned Independently to Direction of Movement in Light or Dark

To examine the basis for HOM direction encoding in V1, we compared peak responses of single units to opposing HOM directions (Figure 5). Large fractions of individual units responded differentially to opposing HOM directions (Figures 5A and 5B). For a subset of our recordings, single units (n = 128) were tracked across dark and light sessions (Figure S4). Units recorded across

Please cite this article in press as: Guitchounts et al., Encoding of 3D Head Orienting Movements in the Primary Visual Cortex, Neuron (2020), https://doi.org/10.1016/j.neuron.2020.07.014

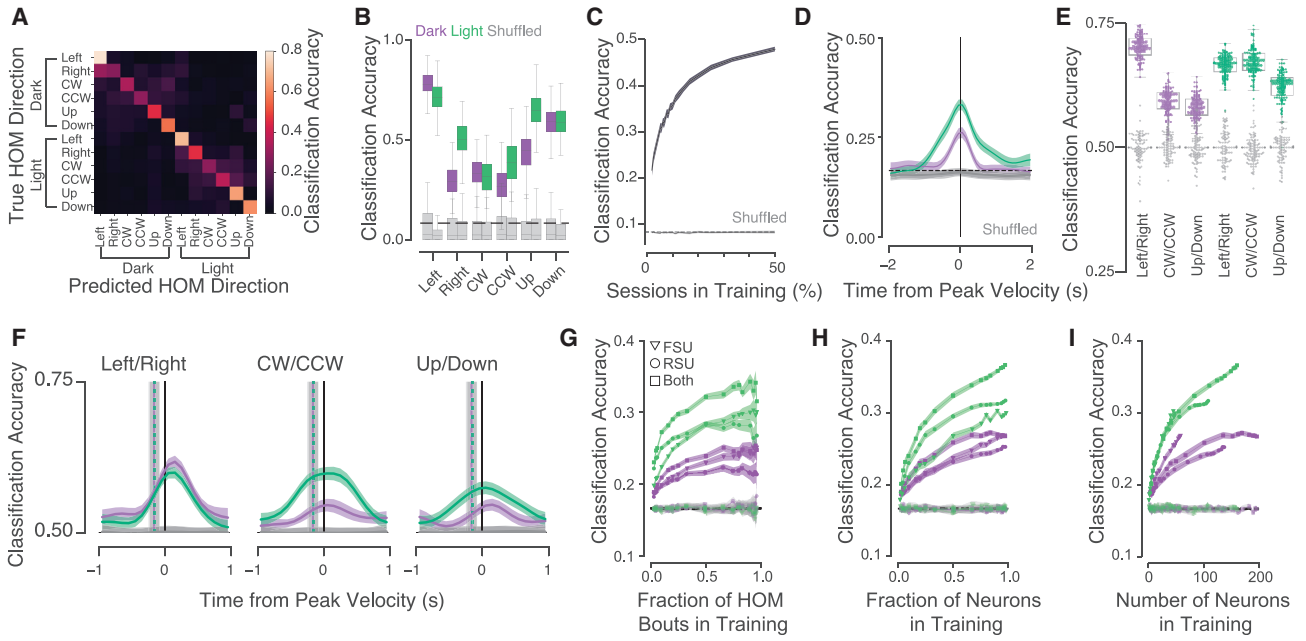

Figure 4. V1 Responses in the Light and Dark Encode Direction of 3D HOMs

(A) Confusion matrix from logistic regression model trained to predict HOM direction from V1 MUA firing rates.

(B) Classification accuracy for different HOM directions in the dark (purple), light (green), and for models trained on shuffled data (gray). Dotted line: chance performance is shown (1/12).

(C) HOM direction decoding performance as a function of the number of sessions used in model training.

(D) Decoding performance as a function of the lag of the training/testing window relative to peak velocity of the head (100-ms non-overlapping bins).

(E) Logistic regression model trained to discriminate left/right, CW/CCW, or up/down HOMs from single-unit activity (RSU and FSU pooled). Performance was on average somewhat lower in the dark (0.62 ± 0.0035 [mean ± SEM]) than in light (0.65 ± 0.0020; $p = 3.2 \times 10^{-12}$, Mann-Whitney U (MWU) test) but mixed for individual HOM directions: left/right (dark: 0.70 ± 0.0023; light: 0.66 ± 0.0022; $p = 4.1 \times 10^{-21}$), CW/CCW (dark: 0.59 ± 0.0026; light: 0.67 ± 0.0027; $p = 4.3 \times 10^{-33}$), up/down (dark: 0.58 ± 0.0024; light: 0.62 ± 0.0029; $p = 3 \times 10^{-20}$). Gray, performance of models trained with shuffled labels. Chance performance = 0.5.

(F) Mean pairwise decoding accuracy as a function of decoding time window (100-ms sliding window) averaged across HOM directions for models trained to discriminate left and right, CW and CCW, or up and down HOM directions. Green and purple vertical lines indicate mean HOM onset times in light and dark, respectively (gray shading: ± 1 SD). Gray horizontal lines and shading, performance of decoder trained on shuffled labels. Chance performance = 0.5.

(G) Classification accuracies for models trained on varying fractions of HOM bouts, from n = 100 total bouts, split by neuron types.

(H) Classification accuracies for models trained on varying fractions of neurons.

(I) Same as (H) but plotted as a function of the number of neurons used rather than the fraction.

See also Figure S4.

light and dark responded differently to the same HOM direction in the opposing lighting conditions (Figure 5C). Further, units were tuned to HOM direction at a rate above chance, with about half of cells tuned to any particular direction in either lighting condition (Figure 5D).

Units tracked across both lighting conditions allowed us to investigate the relationship between the direction tuning of individual V1 neurons in dark and light. Surprisingly, there was no significant correlation between a cell's direction tuning in the dark and in the light (Figure 5E). Of the cells tuned to HOM direction in either dark or light, fewer than 25% were tuned in both conditions. Observed fractions of neurons tuned to direction in both light and dark were consistent with what could be expected by chance, as indicated by a shuffle analysis (Figure 5F). HOM-direction-tuned neurons in V1, therefore, constituted largely independent populations: one that was tuned to direction in the absence of visual cues (in the dark) and one that was tuned to direction when both visual and motor cues were available (in the light).

V1 Responses to Visual Stimulation Are Suppressed by Orienting Movements and Enhanced by Overall Movement

In freely behaving animals, visual stimuli are processed during both stillness and movement. However, presenting well-controlled visual stimuli to freely moving animals is a challenge, and few studies have measured responses of V1 neurons in unrestrained animals (Meyer et al., 2018; Haggerty and Ji, 2015; Sawinski et al., 2009; Okun et al., 2016). We wanted to know how responses to visual stimulation would be affected by HOMs, reasoning that, if HOMs suppress V1 activity on average, responses to visual stimuli during those movements may be suppressed relative to responses during rest. Alternatively, visual stimulation during HOMs could enhance visual responses, as running does in head-fixed mice (Niell and Stryker, 2010; Polack et al., 2013).

To explore the possibility that HOMs might be associated with altered visual responses, we flashed the behavioral arena light-emitting diode (LED) lights (on for 500 ms, off for a uniformly

Please cite this article in press as: Guitchounts et al., Encoding of 3D Head Orienting Movements in the Primary Visual Cortex, Neuron (2020), https://doi.org/10.1016/j.neuron.2020.07.014

CellPress

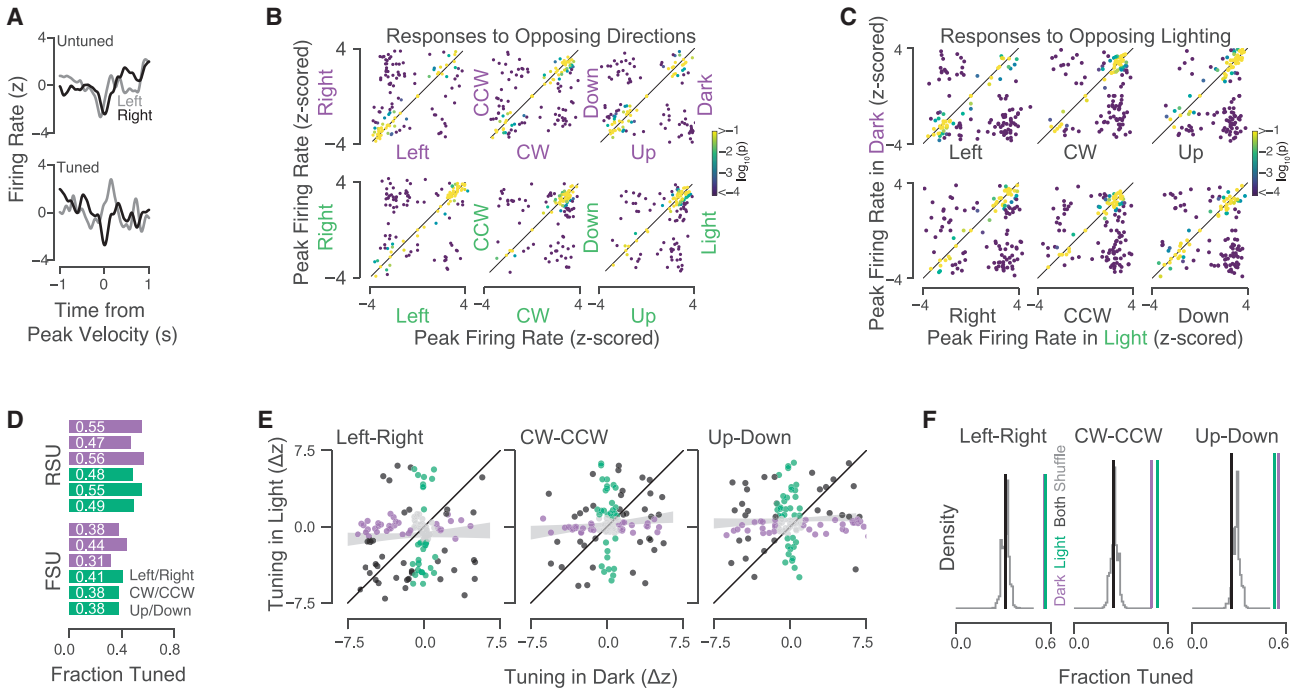

Figure 5. V1 Neurons Are Direction Tuned Independently in Light or Dark

(A) Two example neurons showing mean responses aligned to left (gray) and right (black) HOMs in the dark. One had similar responses to left and right HOMs (top), and the other was suppressed during right HOMs and excited during left HOMs (bottom).

(B) Peak responses of neurons (dots) to opposing HOM directions. Similar responses to opposing directions fall along the diagonal. Off-diagonal responses indicate a cell is tuned to HOM direction. Color indicates probability of the responses to the two directions being different from one another (p value of shuffle test). RSUs and FSUs pooled.

(C) Peak responses of neurons to opposing lighting conditions, split by HOM direction.

(D) Fractions of neurons significantly tuned to HOM direction, split by directions (significance at $p < 0.05$; Bonferroni corrected).

(E) Direction tuning in light and dark for neurons recorded in both lighting conditions. Tuning in one condition did not predict tuning in the other (left-right $r = 0.06$, $p = 0.51$; CW-CCW $r = 0.11$, $p = 0.21$; up-down $r = 0.06$, $p = 0.48$). Green, neurons tuned in light; purple, in dark; black, in both lighting conditions; gray, in neither. Gray shading, correlation ± bootstrap SD.

(F) Fractions of direction-tuned cells in light (green), dark (purple), and both dark and light (black) alongside a distribution density (gray) of shuffled direction tunings. Neurons were direction tuned in both lighting conditions at rates expected if there was no relationship between dark and light tuning: fraction tuned to left-right in dark and light: 0.31, compared to shuffle: $p = 0.44$; fraction tuned to CW-CCW in dark and light: 0.25, compared to shuffle $p = 0.50$; and fraction tuned to up-down in dark and light: 0.25, compared to shuffle $p = 0.86$.

random time 400–600 ms) while the rats were behaving freely and examined average responses during overall movement, HOMs, or rest (Figures 6A and 6B). We hypothesized that V1 receives a suppressive signal during orienting movements, which we unmask by recording in complete darkness and could probe its effect on visual responses by providing a visual stimulus during orienting movements. As such, the arena and experimental room were in darkness when the LEDs were off.

Flash trials were analyzed according to the animals' movement in the 100-ms period after stimulus onset, splitting the data into resting, moving, or orienting trials (see Method Details). Rats spent large fractions of time moving during the flash sessions, with many sub-second bouts of rest and movement, which led us to conclude that the animals were likely not asleep during visual stimulation; this allowed us to compare visual responses in resting or moving animals (Figure 6C). Relative to responses to flashes during rest, MUA firing rates were higher during overall movement and lower during HOMs (Figures 6D and 6E). Thus, V1 responses to visual stimuli were differentially affected by different types of movements, with overall movement being associated with an increase and HOMs with a decrease, respectively, in the gain of responses to visual stimulation.

We next asked how single units responded to flash stimuli (Figure 6F). Responses to flashes were largest when the animals were resting and were suppressed during HOMs, to a greater extent in excitatory than inhibitory cells (Figures 6G–6I). Although peak responses to visual stimulation were lower during HOMs than rest, the activity also persisted longer (Figure 6I). The finding that V1 visual responses are suppressed during orienting movements of the head supports the idea that the rodent visual system may decrease the responsiveness of visually responsive neurons as part of corollary discharge signaling, akin to previous findings in rodent auditory cortex (Schneider et al., 2014, 2018; Rummell et al., 2016) and primate visual areas (Niemeyer and Paradiso, 2018; Sylvester et al., 2005; McFarland et al., 2015; Thiele et al., 2002; Wurtz and Sommer, 2004).

Please cite this article in press as: Guitchounts et al., Encoding of 3D Head Orienting Movements in the Primary Visual Cortex, Neuron (2020), https://doi.org/10.1016/j.neuron.2020.07.014

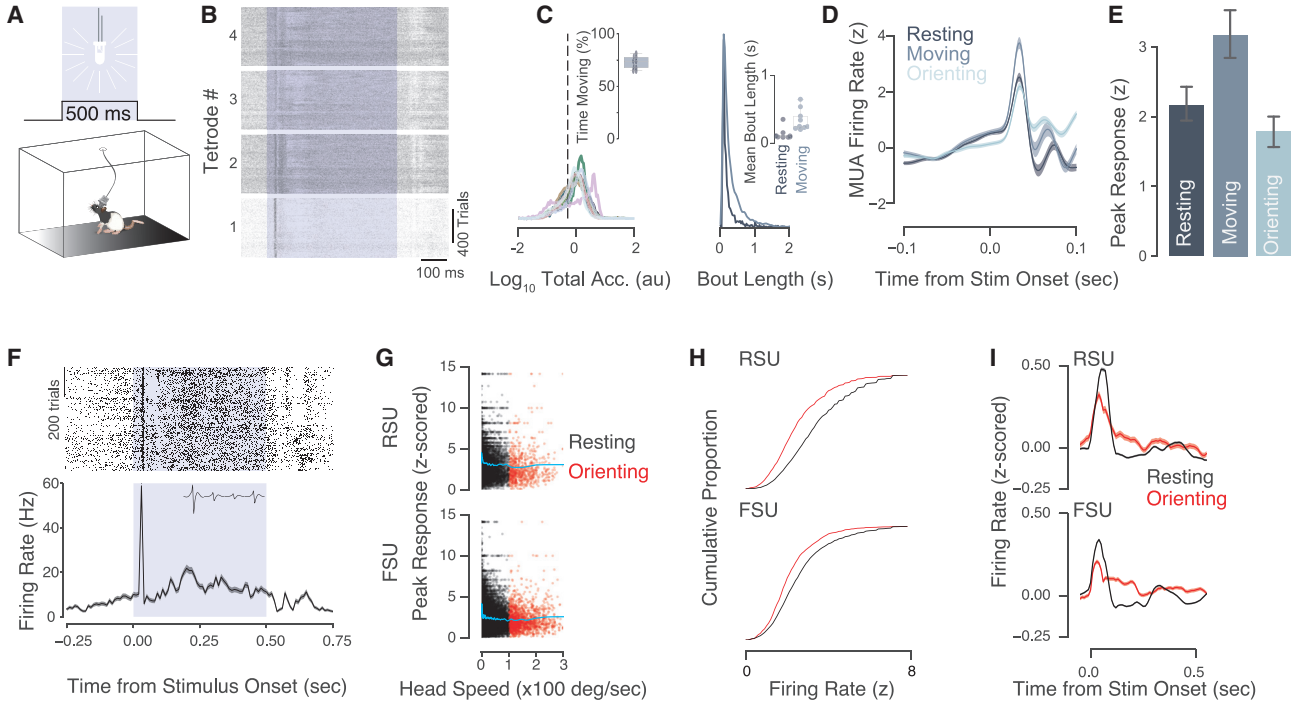

Figure 6. Bidirectional Modulation of V1 Responses to Visual Stimulation during Overall Movement and HOMs

(A) Visual stimuli were presented as 500-ms flashes of the overhead cage lights over the course of several hundred trials.

(B) Response profile of multiunit spikes from four tetrodes from one session. Purple shading represents stimulus timing.

(C) Movement statistics indicate that the rats spent a large fraction of time during light flash sessions moving and alternating between bouts of movement and rest. Left: density of overall movement (total acceleration) for n = 9 sessions among n = 3 rats (each line is one session) is shown. Inset: the rats spent a majority of time (~70%) moving. Right: density of resting and moving bout lengths across sessions is shown. Inset: mean resting and moving bout lengths for each session are shown.

(D) Mean *Z*-scored MUA responses across rats and sessions during light flashes presented during rest, general movement, or head orienting. Shading, SEM.

(E) Mean peak responses after flash onset were higher during general movement (3.17 ± 0.18; mean ± SEM) than rest (2.16 ± 0.12; $p = 7.23 \times 10^{-10}$; t test) or head orienting (1.79 ± 0.12; $p = 1.05 \times 10^{-22}$; t test). Responses during orienting movements were suppressed relative to rest as well ($p = 6.5 \times 10^{-3}$).

(F) Response profile of one V1 cell over n = 707 trials, with spike raster plot (top) and mean ± SEM response (bottom). Inset: waveform of the example unit is shown.

(G) Peak responses to flash stimuli as a function of head speed. Trials are colored by movement condition: resting (black) or orienting (red), with orienting defined as the angular velocity of the head exceeding 100°/s. Each dot is one trial (n = 9,692 trials from n = 52 RSUs and n = 20,439 trials from n = 52 FSUs from n = 12 sessions with n = 656.58 ± 135.76 trials each, across n = 3 rats). Cyan lines indicate the rolling mean.

(H) Cumulative proportion of peak firing rates in the response window.

(I) Mean responses of RSUs (top) and FSUs (bottom) in resting or orienting conditions. Responses were lower during HOMs in RSUs ($p = 4.4 \times 10^{-19}$ MWU test) and FSUs ($p = 1.8 \times 10^{-30}$ MWU test).

V1 Head-Orienting Responses Depend on M2

The observation that V1 responded to HOMs in the dark before HOM onset suggests that HOM-related signals in V1 might originate in a motor region of the brain. A multitude of anatomical, functional, and electrophysiological evidence pointed to M2 as a likely source of HOM signals in V1. We therefore lesioned large portions of M2 (including the area that projects to V1) via bilateral injections of ibotenic acid (Figures 7A–7C, S5, and S6A). The lesions did not alter orienting behaviors (Figures 7D, S6B, and S6C); further, MUA firing rates were still higher during overall movement compared to rest, albeit to a lesser extent compared to non-lesioned animals (Figure S6D). V1 activity in lesioned animals responded to visual stimulation (Figures S6E–S6K) but exhibited significantly reduced HOM-related responses (Figure 7E). These trends were consistent across animals and HOM directions (Figure S7A).

Across all HOM directions, the previously observed negative responses in the dark and positive responses in the light were largely diminished in lesioned animals, with the magnitude of responses in the dark reduced more so than the magnitudes of responses in the light (Figure 7F). HOM direction encoding was greatly reduced in models trained and tested on lesioned animals' data (Figure 7G), with most dramatic drops in performance for left, right, clockwise (CW), and counterclockwise (CCW) directions in lesioned animals both in dark and light (Figures S7B and S7C). M2 therefore plays a crucial role in shaping HOM-related responses and HOM direction information in V1.

The reduced HOM direction information in lesioned animals led us to compare the correlation structure among the average MUA traces in lesioned and non-lesioned animals (Figures 7H–7J; see Method Details). Correlations among MUA responses to HOMs in

Please cite this article in press as: Guitchounts et al., Encoding of 3D Head Orienting Movements in the Primary Visual Cortex, Neuron (2020), https://doi.org/10.1016/j.neuron.2020.07.014

CellPress

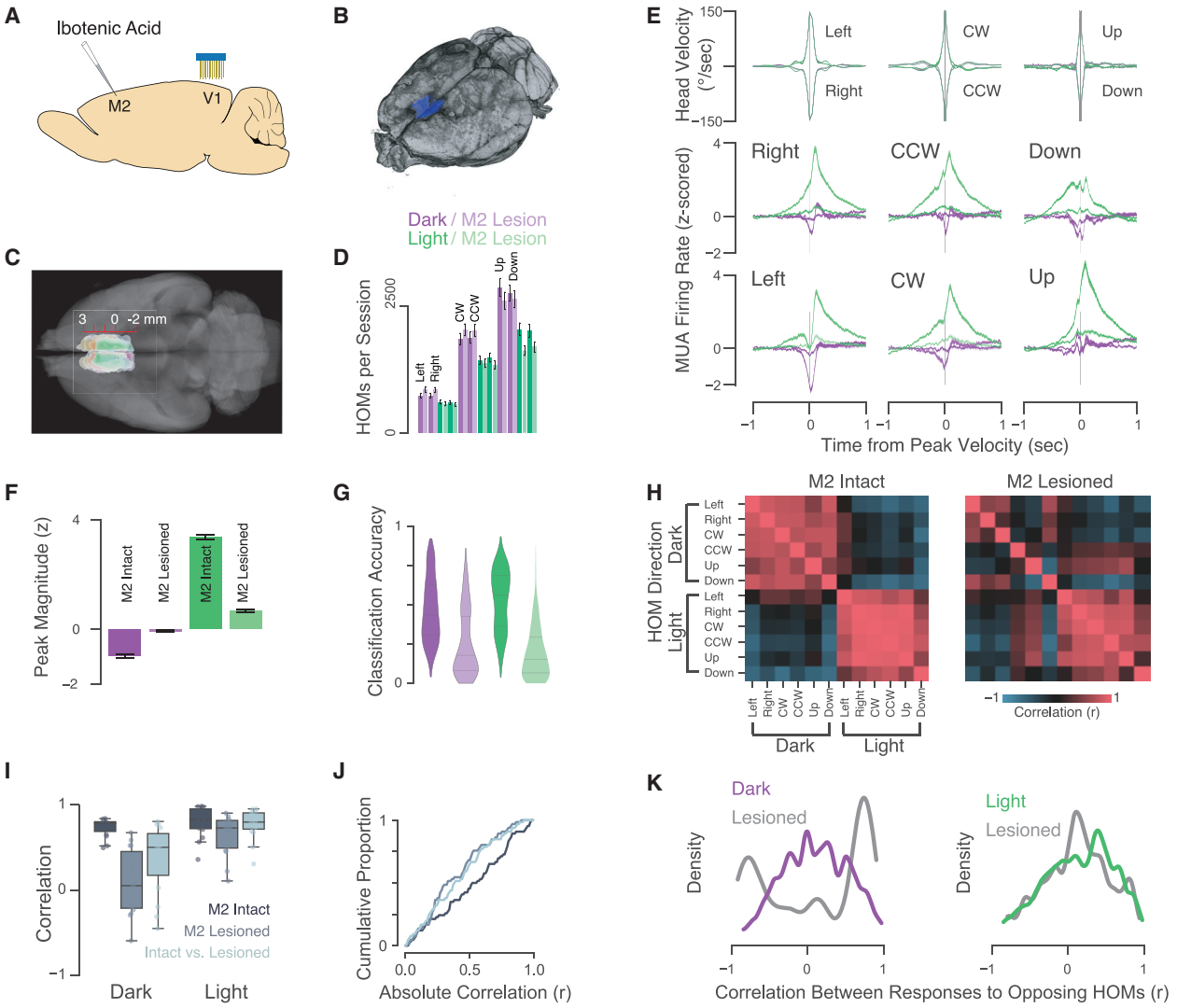

Figure 7. HOM Signals in V1 Depend on Secondary Motor Cortex

(A) M2 was lesioned bilaterally using injections of excitotoxic ibotenic acid. Tetrode arrays were implanted in V1 following lesioning.

(B) An example lesioned brain imaged using micro-CT. Lesion area is highlighted in blue.

(C) Horizontal projection of lesion ROIs (n = 4 rats) overlaid over an example brain. Anterior-posterior coordinates are relative to Bregma.

(D) Numbers of HOMs extracted per session from non-lesioned (darker purple and green) and lesioned rats (lighter purple and green) were indistinguishable from one another (all $p > 0.02$; Mann-Whitney U tests on lesioned versus non-lesioned numbers).

(E) Mean HOM-aligned angular velocities of the head and MUA firing rates across animals and conditions. Top row: extracted HOMs (velocity) are shown. Middle and bottom rows: *Z*-scored MUA firing rates averaged across n = 5 non-lesioned animals, n = 4 lesioned animals, and n = 16 tetrodes each are shown.

(F) Peak MUA magnitudes in the 0.5 s around peak velocity were significantly lower in lesioned rats in the dark ($p < 1.5 \times 10^{-41}$; MWU test) and light ($p < 3.9 \times 10^{-109}$; MWU test).

(G) HOM direction decoding models trained and tested on lesioned animals performed poorly (classification accuracy: 0.26 ± 0.01 for dark; 0.19 ± 0.01 for light) compared to non-lesioned models (0.45 ± 0.01 for dark; 0.53 ± 0.01 for light; mean ± SEM).

(H) Correlation structure of MUA traces among HOM directions in dark and light in non-lesioned (left) and lesioned (right) rats.

(I) Correlations are reduced in lesioned animals, more so in the dark ($r = 0.73 \pm 0.03$ in non-lesioned and $r = 0.10 \pm 0.10$ in lesioned rats $p = 6.5 \times 10^{-4}$; MWU test) than in the light ($r = 0.80 \pm 0.05$ in non-lesioned and $r = 0.65 \pm 0.06$ in lesioned rats $p = 6.5 \times 10^{-4}$; MWU test).

(J) Cumulative proportions of absolute correlations among HOM directions.

(K) Correlation of single-unit responses during opposing (left versus right, CW versus CCW, and up versus down) HOM directions. In the dark, 49.0% of units in lesioned rats highly correlated responses ($r > 0.5$), compared to 20% in non-lesioned rats, and 31.4% had highly anti-correlated responses ($r < -0.5$) compared to 6.2% in non-lesioned rats. Conversely, in the light, 18.7% of units in lesioned rats highly correlated responses ($r > 0.5$), compared to 23.5% in non-lesioned animals; 8.1% of units in lesioned rats had highly anti-correlated responses, similar to the 7.4% of units in non-lesioned animals.

See also Figures S5–S7.

Please cite this article in press as: Guitchounts et al., Encoding of 3D Head Orienting Movements in the Primary Visual Cortex, Neuron (2020), https://doi.org/10.1016/j.neuron.2020.07.014

lesioned rats were reduced in the dark but remained high in the light (Figures 7I and 7J).

Single-unit correlations in non-lesioned animals were broadly distributed both in the dark and light, reflecting a capacity to encode HOM direction (Figure 7K). In contrast, in lesioned animals, over half of the neurons had highly correlated responses to opposing HOM directions in the dark (compared to 20% in non-lesioned animals), and one-third were highly anticorrelated (compared to 6% in non-lesioned animals). Correlation structure in the light appeared to be qualitatively similar between lesioned and non-lesioned animals, likely reflecting common visual drive. These results demonstrate that M2 shapes responses to orienting movements of the head in V1, suggesting that M2 may support a neural mechanism that predicts the direction of visual flow given a motor command and cancels the effects of such flow on sensory processing.

DISCUSSION

Vision has largely been studied in a passive context, with restrained animals passively absorbing stimuli projected on a screen. In their natural states, however, animals interact with sensory stimuli of various modalities by sniffing, whisking or palpating, or making saccadic movements of the eyes, head, or body. Saccadic eye movements in primates have been studied extensively, but although rodents also make complex patterns of movements of the head and eyes, their functional purpose and impact on visual processing is for the most part unknown. We reasoned that recording neuronal activity in V1 of freely behaving rats could help clarify the impact of naturalistic movements on sensory cortical dynamics. We found that V1 dynamics in rats during free movement precisely relate to 3D movements of the head in a manner that depends on secondary motor cortex. V1 multiunit firing rates were suppressed during orienting movements of the head in the dark and enhanced in the light on a sub-second basis. Further, around half of individual neurons were tuned to particular HOM directions in a manner that depended on the presence or absence of light. Our data therefore suggest a framework by which cortex can distinguish self-generated sensory signals and those that come from the outside world; these findings further raise the possibility that orienting movements of the head serve the same functional purpose in rodents as saccadic eye movements do in primates.

Movement-related neuronal activity has been found across virtually all regions of the mammalian brain, but its function remains unknown (Stringer et al., 2019; Musall et al., 2019). Locomotion signals in V1 have been proposed to predict visual flow direction (Vélez-Fort et al., 2018; Leinweber et al., 2017); such signals could support a predictive coding framework in which V1 computes deviations from expected flow, thereby making long-range communication among visual areas more efficient (Keller et al., 2012; Keller and Mrsic-Flogel, 2018; Rao and Ballard, 1999). Consistent with this theory's prescription for positive and negative prediction error units (Keller and Mrsic-Flogel, 2018), our data showed V1 single units to respond bidirectionally to HOMs in the presence or absence of visual cues (Figure 5C).

An idea related to the predictive coding theory is that movement signals in sensory cortex could reflect efference copy signals from motor regions. Such movement signals have been identified in the rodent auditory system and other sensory systems (Schneider et al., 2014; Keller and Hahnloser, 2009; Kennedy et al., 2014; Wurtz and Sommer, 2004; Thiele et al., 2002; Turner-Evans et al., 2017; Kim et al., 2015). Although a signal predicting visual flow and an efference copy of movement plans are similar in nature, the latter could be used to cancel the effects of purposive movement on sensory processing by suppressing activity during movement. Our observation that V1 multiunit and the majority of single units were suppressed in the dark suggests that V1 dynamics reflect not just a prediction of visual flow but also possibly a cancellation of the effects of flow on sensory processing. Further, the fact that V1 dynamics were modulated in an HOM-direction-specific manner suggests that the predictions reflect specific 3D movement dynamics.

Further, responses of V1 single units to visual stimulation were diminished during HOMs compared to rest. These data are reminiscent of the suppression of activity observed in auditory cortex during locomotion but stand in contrast with the enhanced neural responses observed in visual cortex during locomotion (Niell and Stryker, 2010; Polack et al., 2013; Saleem et al., 2013; Vinck et al., 2015; Ayaz et al., 2013). One possible explanation of this discrepancy is that running and orienting movements produce opposing effects on visual responses. Forward locomotion and orienting movements of the head produce distinct types of optic flow: the former is accompanied by translational velocity fields although the latter produces rotational fields (Warren and Hannon, 1990). Our data show that overall movement and HOMs produced distinct effects on V1 activity, with a net enhancement during overall movement and suppression during HOMs (Figures 2 and 3). The enhancing effects of general movement on V1 activity have been previously observed in head-fixed mice running on treadmills (Niell and Stryker, 2010; Fu et al., 2014; Polack et al., 2013; Saleem et al., 2013; Keller et al., 2012); effects of passive head rotations have been reported as well (Vélez-Fort et al., 2018; Bouvier et al., 2020).

Lesions to M2 severely diminished HOM-related activity while sparing the orienting behaviors (Figure 7) and preserving responses to visual stimulation (Figures S6E–S6K). Although M2 axons project directly to V1 (Figure S5; Leinweber et al., 2017), it is possible that HOM-related activity in V1 is not directly inherited from axonal projections from M2 but from M2's influence on retrosplenial cortex (RSC) (Vélez-Fort et al., 2018) or thalamic nuclei (Roth et al., 2016). It is also possible that V1 inherits HOM-related signals from the lateral geniculate nucleus (LGN), which has been shown to be affected by locomotion (Erisken et al., 2014). Finally, the present work does not address why lesioning M2 spares production of HOMs, even though previous studies have implicated this region in controlling orienting movements of the head and eyes (Sinnamon and Galer, 1984; Hall and Lindholm, 1974; Itokazu et al., 2018). It is possible that this discrepancy is due to the fact that the previous studies used micro-stimulation to elicit eye or head movements, which could indicate that M2's control of such movements is indirect or modulatory

in nature (Otchy et al., 2015). Further elucidation of the movement signal pathways of M2 and V1 will require genetic tools to silence or record the dynamics of M2-projecting axons over V1 in a freely behaving context (Leinweber et al., 2017).

A major challenge for studying vision in unrestrained animals is the control of visual stimulation, a problem that might be solved using head-mounted LED screens or cameras (Wallace et al., 2013). Recent work in head-fixed mice running in virtual reality (VR), where visual flow is yoked to locomotion, represents an important advance in studying vision as an active sensation (Harvey et al., 2009; Keller et al., 2012; Saleem et al., 2018; Leinweber et al., 2017). Still, most VR setups require head restraint, which prevents naturalistic interaction with visual stimuli.

Our data show that various orienting movements in 3D have profound effects on neuronal dynamics in V1, a cortical area traditionally thought to primarily perform feedforward computations on incoming visual information. Although the 3D movements examined here are closer to naturalistic behavior than locomotion in restrained animals, the characterization of free movement as HOMs along three axes is still lacking compared to the complex patterns of movement animals actually perform. Another caveat in the present work is that the head-mounted IMU data are agnostic to whisker movements; as such, it is possible that some whisker movements could have affected V1 activity. It will therefore be critical to continue examining sensory cortical dynamics using computational neuroethology methods that reveal the structure of naturalistic behavior and measure as many relevant motor variables as possible (Markowitz et al., 2018).

Saccadic eye movements in primates serve to shift gaze, foveate, and explore a visual scene. These movements are accompanied by a suppression of activity in visual brain areas, which serves to reduce blur. Rodents make complex patterns of head and eye movements, some of which are used to estimate distances, but whether or not these also serve to explore a visual scene—a retinal palpation—is not clear because the rodent retina does not have a fovea. Our finding that V1 activity is suppressed during orienting movements of the head, just as primate visual areas are suppressed during saccades, raises two intriguing possibilities: that such orienting movements serve the same functional purpose in rats that saccades do in primates and that the circuitry for implementing this important computation evolved first in afoveate animals. Finally, our findings are consistent with a model in which sensation and action are deeply intertwined processes: animals actively sample the sensory world in order to make decisions and learn. Understanding vision therefore will be facilitated by considering it an active process and exploring its underlying neural codes while subjects are free to behave.

STAR★METHODS

Detailed methods are provided in the online version of this paper and include the following:

SUPPLEMENTAL INFORMATION

Supplemental Information can be found online at https://doi.org/10.1016/j.neuron.2020.07.014.

ACKNOWLEDGMENTS

We would like to thank Jeffrey Markowitz, Bence Ölveczky, Sandeep Robert Datta, and Juliana Rhee for advice and helpful comments on the manuscript. We thank Gerald Pho for providing ibotenic acid and advice on lesion segmentation. Edward Soucy, Brett Graham, and Joel Greenwood of the CBS Neuroengineering Core were instrumentally helpful in technical advice and on light measurements. Douglas Richardson of the Harvard Center for Biological Imaging helped with slice imaging. H. Greg Lin of the Harvard Center for Nanoscale Systems assisted with micro-computed tomography (CT) imaging. This work was performed in part at the Center for Nanoscale Systems (CNS), a member of the National Nanotechnology Coordinated Infrastructure Network (NNCI), which is supported by the National Science Foundation under NSF award no. 1541959. CNS is part of Harvard University. S.B.E.W. was supported by EMBO and HFSP postdoctoral fellowships. G.G. was supported by the National Science Foundation (NSF) Graduate Research Fellowship Program (GRFP).

AUTHOR CONTRIBUTIONS

G.G. conceived and performed the electrophysiology experiments, analyzed the data, and wrote the manuscript. S.B.E.W. designed the viral tracing and lesion experiments. J.M. designed and performed the micro-CT and osmium staining experiments. D.C. provided research funding and space.

DECLARATION OF INTERESTS

The authors declare no competing interests.

Received: March 5, 2020
Revised: June 11, 2020
Accepted: July 13, 2020
Published: August 11, 2020

REFERENCES

Ayaz, A., Saleem, A.B., Schölvinck, M.L., and Carandini, M. (2013). Locomotion controls spatial integration in mouse visual cortex. Curr. Biol. *23*, 890–894.

Barth, T.M., Parker, S.M., and Sinnamon, H.M. (1982). Unilateral lesions of the anteromedial cortex in the rat impair approach to contralateral visual cues. Physiol. Behav. *29*, 141–147.

Barthas, F., and Kwan, A.C. (2017). Secondary motor cortex: where 'sensory' meets 'motor' in the rodent frontal cortex. Trends Neurosci. *40*, 181–193.

Binda, P., and Morrone, M.C. (2018). Vision during saccadic eye movements. Annu. Rev. Vis. Sci. *4*, 193–213.

Bouvier, G., Senzai, Y., and Scanziani, M. (2020). Head movements control the activity of primary visual cortex in a luminance dependent manner. bioRxiv. https://doi.org/10.1101/2020.01.20.913160.

Chung, J.E., Magland, J.F., Barnett, A.H., Tolosa, V.M., Tooker, A.C., Lee, K.Y., Shah, K.G., Felix, S.H., Frank, L.M., and Greengard, L.F. (2017). A fully automated approach to spike sorting. Neuron *95*, 1381–1394.e6.

Clancy, K.B., Orsolic, I., and Mrsic-Flogel, T.D. (2019). Locomotion-dependent remapping of distributed cortical networks. Nat. Neurosci. *22*, 778–786.

Crapse, T.B., and Sommer, M.A. (2008). Corollary discharge across the animal kingdom. Nat. Rev. Neurosci. *9*, 587–600.

Cullen, K.E. (2019). Vestibular processing during natural self-motion: implications for perception and action. Nat. Rev. Neurosci. *20*, 346–363.

Dhawale, A.K., Poddar, R., Wolff, S.B., Normand, V.A., Kopelowitz, E., and Ölveczky, B.P. (2017). Automated long-term recording and analysis of neural activity in behaving animals. eLife *6*, 91.

DiCarlo, J.J., and Cox, D.D. (2007). Untangling invariant object recognition. Trends Cogn. Sci. *11*, 333–341.

Donoghue, J.P., and Wise, S.P. (1982). The motor cortex of the rat: cytoarchitecture and microstimulation mapping. J. Comp. Neurol. *212*, 76–88.

Ellard, C.G., Goodale, M.A., and Timney, B. (1984). Distance estimation in the Mongolian gerbil: the role of dynamic depth cues. Behav. Brain Res. *14*, 29–39.

Erisken, S., Vaiceliunaite, A., Jurjut, O., Fiorini, M., Katzner, S., and Busse, L. (2014). Effects of locomotion extend throughout the mouse early visual system. Curr. Biol. *24*, 2899–2907.

Erlich, J.C., Bialek, M., and Brody, C.D. (2011). A cortical substrate for memory-guided orienting in the rat. Neuron *72*, 330–343.

Felleman, D.J., and Van Essen, D.C. (1991). Distributed hierarchical processing in the primate cerebral cortex. Cereb. Cortex *1*, 1–47.

Ferguson, J.E., Boldt, C., and Redish, A.D. (2009). Creating low-impedance tetrodes by electroplating with additives. Sens. Actuators A Phys. *156*, 388–393.

Fu, Y., Tucciarone, J.M., Espinosa, J.S., Sheng, N., Darcy, D.P., Nicoll, R.A., Huang, Z.J., and Stryker, M.P. (2014). A cortical circuit for gain control by behavioral state. Cell *156*, 1139–1152.

Gabbott, P.L., Warner, T.A., Jays, P.R., Salway, P., and Busby, S.J. (2005). Prefrontal cortex in the rat: projections to subcortical autonomic, motor, and limbic centers. J. Comp. Neurol. *492*, 145–177.

Haggerty, D.C., and Ji, D. (2015). Activities of visual cortical and hippocampal neurons co-fluctuate in freely moving rats during spatial behavior. eLife *4*, e08902.

Hagins, W.A., Penn, R.D., and Yoshikami, S. (1970). Dark current and photocurrent in retinal rods. Biophys. J. *10*, 380–412.

Hall, R.D., and Lindholm, E.P. (1974). Organization of motor and somatosensory neocortex in the albino rat. Brain Res. *66*, 23–38.

Harvey, C.D., Collman, F., Dombeck, D.A., and Tank, D.W. (2009). Intracellular dynamics of hippocampal place cells during virtual navigation. Nature *461*, 941–946.

Hengen, K.B., Torrado Pacheco, A., McGregor, J.N., Van Hooser, S.D., and Turrigiano, G.G. (2016). Neuronal firing rate homeostasis is inhibited by sleep and promoted by wake. Cell *165*, 180–191.

Hoy, J.L., Yavorska, I., Wehr, M., and Niell, C.M. (2016). Vision drives accurate approach behavior during prey capture in laboratory mice. Curr. Biol. *26*, 3046–3052.

Hubel, D.H., and Wiesel, T.N. (1962). Receptive fields, binocular interaction and functional architecture in the cat's visual cortex. J. Physiol. *160*, 106–154.

Itokazu, T., Hasegawa, M., Kimura, R., Osaki, H., Albrecht, U.R., Sohya, K., Chakrabarti, S., Itoh, H., Ito, T., Sato, T.K., and Sato, T.R. (2018). Streamlined sensory motor communication through cortical reciprocal connectivity in a visually guided eye movement task. Nat. Commun. *9*, 338.

Kanki, J.P., Martin, T.L., and Sinnamon, H.M. (1983). Activity of neurons in the anteromedial cortex during rewarding brain stimulation, saccharin consumption and orienting behavior. Behav. Brain Res. *8*, 69–84.

Keller, G.B., and Hahnloser, R.H. (2009). Neural processing of auditory feedback during vocal practice in a songbird. Nature *457*, 187–190.

Keller, G.B., and Mrsic-Flogel, T.D. (2018). Predictive processing: a canonical cortical computation. Neuron *100*, 424–435.

Keller, G.B., Bonhoeffer, T., and Hübener, M. (2012). Sensorimotor mismatch signals in primary visual cortex of the behaving mouse. Neuron *74*, 809–815.

Kennedy, A., Wayne, G., Kaifosh, P., Alviña, K., Abbott, L.F., and Sawtell, N.B. (2014). A temporal basis for predicting the sensory consequences of motor commands in an electric fish. Nat. Neurosci. *17*, 416–422.

Kim, A.J., Fitzgerald, J.K., and Maimon, G. (2015). Cellular evidence for efference copy in Drosophila visuomotor processing. Nat. Neurosci. *18*, 1247–1255.

Kloosterman, F., Davidson, T.J., Gomperts, S.N., Layton, S.P., Hale, G., Nguyen, D.P., and Wilson, M.A. (2009). Micro-drive array for chronic in vivo recording: drive fabrication. J. Vis. Exp. 1094.

Kral, K. (2003). Behavioural-analytical studies of the role of head movements in depth perception in insects, birds and mammals. Behav. Processes *64*, 1–12.

Krock, R.M., and Moore, T. (2014). The influence of gaze control on visual perception: eye movements and visual stability. Cold Spring Harb. Symp. Quant. Biol. *79*, 123–130.

Land, M.F. (1999). Motion and vision: why animals move their eyes. J. Comp. Physiol. A Neuroethol. Sens. Neural Behav. Physiol. *185*, 341–352.

Land, M.F. (2015). Eye movements of vertebrates and their relation to eye form and function. J. Comp. Physiol. A Neuroethol. Sens. Neural Behav. Physiol. *201*, 195–214.

Legg, C.R., and Lambert, S. (1990). Distance estimation in the hooded rat: experimental evidence for the role of motion cues. Behav. Brain Res. *41*, 11–20.

Leichnetz, G.R., Hardy, S.G., and Carruth, M.K. (1987). Frontal projections to the region of the oculomotor complex in the rat: a retrograde and anterograde HRP study. J. Comp. Neurol. *263*, 387–399.

Leinweber, M., Ward, D.R., Sobczak, J.M., Attinger, A., and Keller, G.B. (2017). A sensorimotor circuit in mouse cortex for visual flow predictions. Neuron *95*, 1420–1432.e5.

Leonard, C.M. (1969). The prefrontal cortex of the rat. I. Cortical projection of the mediodorsal nucleus. II. Efferent connections. Brain Res. *12*, 321–343.

Madisen, L., Garner, A.R., Shimaoka, D., Chuong, A.S., Klapoetke, N.C., Li, L., van der Bourg, A., Niino, Y., Egolf, L., Monetti, C., et al. (2015). Transgenic mice for intersectional targeting of neural sensors and effectors with high specificity and performance. Neuron *85*, 942–958.

Markowitz, J.E., Gillis, W.F., Beron, C.C., Neufeld, S.Q., Robertson, K., Bhagat, N.D., Peterson, R.E., Peterson, E., Hyun, M., Linderman, S.W., et al. (2018). The striatum organizes 3D behavior via moment-to-moment action selection. Cell *174*, 44–58.e17.

Masis, J., Mankus, D., Wolff, S.B.E., Guitchounts, G., Joesch, M., and Cox, D.D. (2018a). A micro-CT-based method for characterizing lesions and locating electrodes in small animal brains. J. Vis. Exp. 58585.

Masís, J., Mankus, D., Wolff, S.B.E., Guitchounts, G., Joesch, M., and Cox, D.D. (2018b). A micro-CT-based method for quantitative brain lesion characterization and electrode localization. Sci. Rep. *8*, 5184.

McFarland, J.M., Bondy, A.G., Saunders, R.C., Cumming, B.G., and Butts, D.A. (2015). Saccadic modulation of stimulus processing in primary visual cortex. Nat. Commun. *6*, 8110.

Meister, M., and Cox, D. (2013). Rats maintain a binocular field centered on the horizon. F1000Res. *2*, 176.

Mendoza, G., Peyrache, A., Gámez, J., Prado, L., Buzsáki, G., and Merchant, H. (2016). Recording extracellular neural activity in the behaving monkey using

a semichronic and high-density electrode system. J. Neurophysiol. *116*, 563–574.

Meyer, A.F., Poort, J., O'Keefe, J., Sahani, M., and Linden, J.F. (2018). A head-mounted camera system integrates detailed behavioral monitoring with multichannel electrophysiology in freely moving mice. Neuron *100*, 46–60.e7.

Miller, K.D. (2016). Canonical computations of cerebral cortex. Curr. Opin. Neurobiol. *37*, 75–84.

Mimica, B., Dunn, B.A., Tombaz, T., Bojja, V.P.T.N.C.S., and Whitlock, J.R. (2018). Efficient cortical coding of 3D posture in freely behaving rats. Science *362*, 584–589.

Mohler, C.W., and Cechner, R. (1975). Saccadic suppression in the monkey. Vision Res. *15*, 1157–1160.

Morris, A.P., and Krekelberg, B. (2019). A stable visual world in primate primary visual cortex. Curr. Biol. *29*, 1471–1480.e6.

Musall, S., Kaufman, M.T., Juavinett, A.L., Gluf, S., and Churchland, A.K. (2019). Single-trial neural dynamics are dominated by richly varied movements. Nat. Neurosci. *22*, 1677–1686.

Nguyen, D.P., Layton, S.P., Hale, G., Gomperts, S.N., Davidson, T.J., Kloosterman, F., and Wilson, M.A. (2009). Micro-drive array for chronic in vivo recording: tetrode assembly. J. Vis. Exp. 1098.

Niell, C.M., and Stryker, M.P. (2010). Modulation of visual responses by behavioral state in mouse visual cortex. Neuron *65*, 472–479.

Niemeyer, J.E., and Paradiso, M.A. (2018). Saccade-based termination responses in macaque V1 and visual perception. Vis. Neurosci. *35*, E025.

Nymark, S., Heikkinen, H., Haldin, C., Donner, K., and Koskelainen, A. (2005). Light responses and light adaptation in rat retinal rods at different temperatures. J. Physiol. *567*, 923–938.

Okun, M., Lak, A., Carandini, M., and Harris, K.D. (2016). Long term recordings with immobile silicon probes in the mouse cortex. PLoS ONE *11*, e0151180.

Otchy, T.M., Wolff, S.B., Rhee, J.Y., Pehlevan, C., Kawai, R., Kempf, A., Gobes, S.M., and Ölveczky, B.P. (2015). Acute off-target effects of neural circuit manipulations. Nature *528*, 358–363.

Pedregosa, F., Varoquaux, G., Gramfort, A., Michel, V., Thirion, B., Grisel, O., Blondel, M., Prettenhofer, P., Weiss, R., Dubourg, V., et al. (2011). Scikit-learn: machine learning in python. J. Mach. Learn. Res. *12*, 2825–2830.

Polack, P.O., Friedman, J., and Golshani, P. (2013). Cellular mechanisms of brain state-dependent gain modulation in visual cortex. Nat. Neurosci. *16*, 1331–1339.

Rao, R.P., and Ballard, D.H. (1999). Predictive coding in the visual cortex: a functional interpretation of some extra-classical receptive-field effects. Nat. Neurosci. *2*, 79–87.

Roth, M.M., Dahmen, J.C., Muir, D.R., Imhof, F., Martini, F.J., and Hofer, S.B. (2016). Thalamic nuclei convey diverse contextual information to layer 1 of visual cortex. Nat. Neurosci. *19*, 299–307.

Rummell, B.P., Klee, J.L., and Sigurdsson, T. (2016). Attenuation of responses to self-generated sounds in auditory cortical neurons. J. Neurosci. *36*, 12010–12026.

Sakatani, T., and Isa, T. (2007). Quantitative analysis of spontaneous saccade-like rapid eye movements in C57BL/6 mice. Neurosci. Res. *58*, 324–331.

Saleem, A.B., Ayaz, A., Jeffery, K.J., Harris, K.D., and Carandini, M. (2013). Integration of visual motion and locomotion in mouse visual cortex. Nat. Neurosci. *16*, 1864–1869.

Saleem, A.B., Diamanti, E.M., Fournier, J., Harris, K.D., and Carandini, M. (2018). Coherent encoding of subjective spatial position in visual cortex and hippocampus. Nature *562*, 124–127.

Sawinski, J., Wallace, D.J., Greenberg, D.S., Grossmann, S., Denk, W., and Kerr, J.N. (2009). Visually evoked activity in cortical cells imaged in freely moving animals. Proc. Natl. Acad. Sci. USA *106*, 19557–19562.

Schindelin, J., Arganda-Carreras, I., Frise, E., Kaynig, V., Longair, M., Pietzsch, T., Preibisch, S., Rueden, C., Saalfeld, S., Schmid, B., et al. (2012). Fiji: an open-source platform for biological-image analysis. Nat. Methods *9*, 676–682.

Schneider, D.M., Nelson, A., and Mooney, R. (2014). A synaptic and circuit basis for corollary discharge in the auditory cortex. Nature *513*, 189–194.

Schneider, D.M., Sundararajan, J., and Mooney, R. (2018). A cortical filter that learns to suppress the acoustic consequences of movement. Nature *561*, 391–395.

Siegle, J.H., López, A.C., Patel, Y.A., Abramov, K., Ohayon, S., and Voigts, J. (2017). Open Ephys: an open-source, plugin-based platform for multichannel electrophysiology. J. Neural Eng. *14*, 045003–045014.

Sinnamon, H.M., and Galer, B.S. (1984). Head movements elicited by electrical stimulation of the anteromedial cortex of the rat. Physiol. Behav. *33*, 185–190.

Soucy, E., Wang, Y., Nirenberg, S., Nathans, J., and Meister, M. (1998). A novel signaling pathway from rod photoreceptors to ganglion cells in mammalian retina. Neuron *21*, 481–493.

Stringer, C., Pachitariu, M., Steinmetz, N., Reddy, C.B., Carandini, M., and Harris, K.D. (2019). Spontaneous behaviors drive multidimensional, brainwide activity. Science *364*, 255.

Stuesse, S.L., and Newman, D.B. (1990). Projections from the medial agranular cortex to brain stem visuomotor centers in rats. Exp. Brain Res. *80*, 532–544.

Sylvester, R., Haynes, J.D., and Rees, G. (2005). Saccades differentially modulate human LGN and V1 responses in the presence and absence of visual stimulation. Curr. Biol. *15*, 37–41.

Tafazoli, S., Safaai, H., De Franceschi, G., Rosselli, F.B., Vanzella, W., Riggi, M., Buffolo, F., Panzeri, S., and Zoccolan, D. (2017). Emergence of transformation-tolerant representations of visual objects in rat lateral extrastriate cortex. eLife *6*, e22794.

Thiele, A., Henning, P., Kubischik, M., and Hoffmann, K.P. (2002). Neural mechanisms of saccadic suppression. Science *295*, 2460–2462.

Thilo, K.V., Santoro, L., Walsh, V., and Blakemore, C. (2004). The site of saccadic suppression. Nat. Neurosci. *7*, 13–14.

Timo-Iaria, C., Negrão, N., Schmidek, W.R., Hoshino, K., Lobato de Menezes, C.E., and Leme da Rocha, T. (1970). Phases and states of sleep in the rat. Physiol. Behav. *5*, 1057–1062.

Turner-Evans, D., Wegener, S., Rouault, H., Franconville, R., Wolff, T., Seelig, J.D., Druckmann, S., and Jayaraman, V. (2017). Angular velocity integration in a fly heading circuit. eLife *6*, e23496.

Vandecasteele, M., M, S., Royer, S., Belluscio, M., Berényi, A., Diba, K., Fujisawa, S., Grosmark, A., Mao, D., Mizuseki, K., et al. (2012). Large-scale recording of neurons by movable silicon probes in behaving rodents. J. Vis. Exp. e3568.

Vélez-Fort, M., Bracey, E.F., Keshavarzi, S., Rousseau, C.V., Cossell, L., Lenzi, S.C., Strom, M., and Margrie, T.W. (2018). A circuit for integration of head- and visual-motion signals in layer 6 of mouse primary visual cortex. Neuron *98*, 179–191.e6.

Vinck, M., Batista-Brito, R., Knoblich, U., and Cardin, J.A. (2015). Arousal and locomotion make distinct contributions to cortical activity patterns and visual encoding. Neuron *86*, 740–754.

Wallace, D.J., Greenberg, D.S., Sawinski, J., Rulla, S., Notaro, G., and Kerr, J.N. (2013). Rats maintain an overhead binocular field at the expense of constant fusion. Nature *498*, 65–69.

Warren, W.H., Jr., and Hannon, D.J. (1990). Eye movements and optical flow. J. Opt. Soc. Am. A *7*, 160–169.

Watson, B.O., Levenstein, D., Greene, J.P., Gelinas, J.N., and Buzsáki, G. (2016). Network homeostasis and state dynamics of neocortical sleep. Neuron *90*, 839–852.

Williamson, R.S., Hancock, K.E., Shinn-Cunningham, B.G., and Polley, D.B. (2015). Locomotion and task demands differentially modulate thalamic audiovisual processing during active search. Curr. Biol. *25*, 1885–1891.

Wiltschko, A.B., Johnson, M.J., Iurilli, G., Peterson, R.E., Katon, J.M., Pashkovski, S.L., Abraira, V.E., Adams, R.P., and Datta, S.R. (2015). Mapping sub-second structure in mouse behavior. Neuron *88*, 1121–1135.

Wurtz, R.H., and Sommer, M.A. (2004). Identifying corollary discharges for movement in the primate brain. Prog. Brain Res. *144*, 47–60.

Yarbus, A.L. (1967). Eye Movements and Vision (Plenum).

Yushkevich, P.A., Piven, J., Hazlett, H.C., Smith, R.G., Ho, S., Gee, J.C., and Gerig, G. (2006). User-guided 3D active contour segmentation of anatomical structures: significantly improved efficiency and reliability. Neuroimage *31*, 1116–1128.

Zhang, S., Xu, M., Chang, W.C., Ma, C., Hoang Do, J.P., Jeong, D., Lei, T., Fan, J.L., and Dan, Y. (2016). Organization of long-range inputs and outputs of frontal cortex for top-down control. Nat. Neurosci. *19*, 1733–1742.

Zingg, B., Hintiryan, H., Gou, L., Song, M.Y., Bay, M., Bienkowski, M.S., Foster, N.N., Yamashita, S., Bowman, I., Toga, A.W., and Dong, H.W. (2014). Neural networks of the mouse neocortex. Cell *156*, 1096–1111.

Please cite this article in press as: Guitchounts et al., Encoding of 3D Head Orienting Movements in the Primary Visual Cortex, Neuron (2020), https://doi.org/10.1016/j.neuron.2020.07.014

CellPress

STAR★METHODS

KEY RESOURCES TABLE

REAGENT or RESOURCE	SOURCE	IDENTIFIER
Antibodies		
Rabbit anti-GFP	Life Technologies	AB_221569
Alexa Fluor 488 Goat Anti-Rabbit	Life Technologies	AB_2576217
Chicken Anti-RFP	Sigma	Cat#AB3528
Alexa Fluor 568 Goat Anti-Chicken IgG	Life Technologies	AB_2534098
Bacterial and Virus Strains		
retro-AAV-GFP	Janelia	rAAv2-retro pSyn-Cre
retro-AAV-Cre	Addgene (Madisen et al., 2015)	Cat#51507
AAV-CAG-FLEX-tdTomato	UNC Vector Core	N/A
Chemicals, Peptides, and Recombinant Proteins		
Ibotenic Acid	Abcam	ab120041
Sodium Pentobarbital	Vortech Pharmaceuticals	Cat#9373
Paraformaldehyde	Electron Microscopy Science	Cat#15710
Glutaraldehyde	Electron Microscopy Science	Cat#16220
Osmium	VWR	Cat#19190
Gold Plating Solution	Neuralynx	N/A
Polyethylene glycol (PEG)	VWR	N/A
Experimental Models: Organisms/Strains		
Rats: Long-Evans	Charles River	Strain Code: 006
Software and Algorithms		
Python 3.6	https://www.python.org/	RRID: SCR 008394
Scikit Learn	https://scikit-learn.org/ (Pedregosa et al., 2011)	N/A
Electrophysiology Acquisition Software	(Dhawale et al., 2017)	N/A
Custom Arduino Code	This Paper	N/A
MountainSort	(Chung et al., 2017)	N/A
FIJI	(Schindelin et al., 2012)	N/A
ITK-SNAP	(Yushkevich et al., 2006)	N/A
Other		
IMU	Adafruit	Cat#2472
Teensy 3.2 Microcontroller	Adafruit	Cat#2756
Electrophysiology Acquisition Board	Opal Kelly	Cat#XC6SLX45-2C, 128-MiB
Behavioral Arena LEDs	Amazon	Cat#T93007-1
Electrophysiology Tether	Samtec	SFSD-07-30C-H-12.00-DR-NDS
Electrophysiology Header	Samtec	TFM-107-02-L-D-WT
Commutator	Amazon	Logisaf 22mm 300 Rpm 24 Circuits Capsule Slip Ring 2A 240V Test Equipment
12.5-micron Nichrome Wire	Sandvik-Kanthal	N/A
UMP3 UltraMicroPump	WPI	N/A
Nikon Metrology X-Tek HMX ST 225 Micro-CT scanner	Nikon	N/A

Please cite this article in press as: Guitchounts et al., Encoding of 3D Head Orienting Movements in the Primary Visual Cortex, Neuron (2020), https://doi.org/10.1016/j.neuron.2020.07.014

RESOURCE AVAILABILITY

Lead Contact

Further information and requests for resources and reagents should be directed to and will be fulfilled by the Lead Contact, Grigori Guitchounts (g.guitchounts@gmail.com).

Materials Availability

This study did not generate new unique reagents.

Data and Code Availability

The code generated during this study is available at https://github.com/guitchounts/.

EXPERIMENTAL MODEL AND SUBJECT DETAILS

The care and experimental manipulation of all animals were reviewed and approved by the Harvard Institutional Animal Care and Use Committee. Experimental subjects were female Long Evans rats 3 months or older, weighing 300-500 g ($N = 10$, Charles River, Strain Code: 006).

METHOD DETAILS

Surgery

Rats were implanted with 16-tetrode electrode arrays targeting L2/3 of V1. Animals were anesthetized with 2% isoflurane and placed into a stereotaxic apparatus (Knopf Instruments). Care was taken to clean the scalp with Povidone-iodine swabsticks (Professional Disposables International, #S41125) and isopropyl alcohol (Dynarex #1204) before removing the scalp and cleaning the skull surface with hydrogen peroxide (Swan) and a mixture of citric acid (10%) and ferric chloride (3%) (Parkell #S393). Three to four skull screws (Fine Science Tools, #19010-00) were screwed into the skull to anchor the implant. A 0.003'' stainless steel (A-M Systems, #794700) ground wire was inserted ~2mm tangential to the brain over the cerebellum.

Tetrodes were arrayed in 8x2 grids with ~250-micron spacing, and were implanted in V1 with the long axis spread along the AP (ranging 6-8 mm posterior to bregma, 4.5 mm ML, targeting layer 2/3 at 0.6 mm DV). The dura was glued (Loctite) to the edges of the craniotomy to minimize movement of the brain relative to the electrodes. After electrodes were inserted into the brain, the craniotomy was sealed with Puralube vet ointment (Dechra) and the electrodes were glued down with Metabond (Parkell). Post-operative care included twice-daily injections of buprenex (0.05mg/kg Intraperitoneal (IP)) and dexamethasone (0.5 mg/kg IP) for three days.

Behavior

Spontaneous behavior in rats living in a 15x24'' home cage was recorded under three conditions: dark, in which the lights in the box and room were turned off; light, in which the box was illuminated; and flash, in which visual responsiveness of neurons was assessed by flashing the lights repeatedly (On: 500 ms; Off: 400-600 uniformly random time). Recordings were carried out 24/7 and split into ~2-hour dark and ~2-hour light sessions, with 10-30-minute Flash sessions interspersed in some of the experiments. The animals were housed on a reversed light cycle prior to the experiments.

The behavior box was constructed from aluminum extrusions and black extruded acrylic (McMaster). The floor was covered in bedding and the arena contained a cup with food, a water bottle and toys. The walls were lined with strips of white tape at different orientations to provide visual features in the Light condition, and the box was outfitted with white LED strips (Triangle Bulbs Cool White LED Waterproof Flexible Strip Light, T93007-1, Amazon) to provide illumination. For the Dark condition recordings, room and box lights were turned off and care was taken to make sure most sources of light in the experimental room (e.g., LEDs from computers and other hardware) were covered with black tape. To assess whether the recording box was sufficiently dark, a test was performed with a human subject (GG) acclimated in the room for 30 minutes, after which visual features in the cage were still not visible.

For recordings, rats were tethered with a custom 24'' cable (Samtec, SFSD-07-30C-H-12.00-DR-NDS, TFM-107-02-L-D-WT;McMaster extension spring 9640K123) to a commutator (Logisaf 22mm 300Rpm 24 Circuits Capsule Slip Ring 2A 240V TestEquipment, Amazon). A 9-axis Inertial Measurement Unit (IMU) (BNO055, Adafruit) was used to record movement; the sensor was epoxied to the connector on the cable, in a way that placed it directly above the electrodes and headstage. This not only ensured that the sensor was always in the same position above the animals' heads, but also that it stayed powered after the animals were unplugged, preventing the need to re-calibrate the sensor after each recording. The IMU data were acquired at 100Hz using a micro-controller (Teensy 3.2, Adafruit) and saved directly to the acquisition computer's disk. To synchronize IMU and electrophysiology data, the Teensy provided a 2-bit pseudo-random pulse code to the TTL inputs on the electrophysiology system.

The 9-axis IMU combines signals from a 3-axis accelerometer, 3-axis magnetometer, and 3-axis gyroscope. It is equipped with a data-fusion algorithm that combines the signals to calculate absolute direction in three axes, yielding a vector of yaw, roll, and pitch; in addition, the sensor outputs linear acceleration in the forward/backward, left/right, and up/down directions. The derivatives of the yaw, roll, and pitch signals (which reflect left/right CW/CCW, and up/down angular velocities of the head, respectively), were used to

Please cite this article in press as: Guitchounts et al., Encoding of 3D Head Orienting Movements in the Primary Visual Cortex, Neuron (2020), https://doi.org/10.1016/j.neuron.2020.07.014

assess V1 dynamics during HOMs. To extract HOMs, peaks in crossings of a 100 deg/s threshold of the angular velocity traces were found. The L2 norm of the linear acceleration components was used as a proxy for the overall movement.

Measuring Light Levels in Dark

To assess whether the recording box was sufficiently dark as to prevent the rats from being able to see anything in the dark recordings, we first made sure that it was impossible for a human observer (GG) to see any movement in the recording box after acclimating to the darkened room for 30 minutes. We then attempted to measure photon flux in the box using a photomultiplier tube (PMT) (ET Enterprises #9111B) after amplifying and filtering the signals (12dB lowpass at 10Hz) using a Stanford Research Systems preamplifier (#SR570).

Baseline PMT currents in the darkened behavioral box were measured with the PMT covered by tinfoil. After removing the tinfoil, the PMT current registered at 0.2μA. This corresponds to 0.2×10^{-6} Coulombs/s, which is $0.2\times6.2415\times10^{12}$ electrons/s. Accounting for the PMT's gain of 7.1×10^{6}, that is $(0.2\times6.2415\times10^{12})/(7.1\times10^{6})$ or 1.8×10^{5} photocathode events/s. Given the PMT's 10% quantum efficiency (QE) at 500nm, this corresponds to 1.8×10^{6} photons/s over the PMT's 22mm cross-sectional area, or 80,000 photons/mm/s. Assuming $2.27\mu m^2$ rod cross section (Hagins et al., 1970), 0.4 specific absorption, and QE of 0.34 (Nymark et al., 2005), that is $80000\times2.27\times10^{-6}$ or 0.18 incident photons/rod/s and finally 0.025 R*/rod/s (R*: rhodopsin activations). Based on retinal ganglion cell activity measured in Soucy et al. (1998), 0.025 R*/rod/s would correspond, roughly, to retinal ganglion cells firing at 6.7% of their peak firing rates measured at light levels corresponding to 100 R*/rod/sec.

Electrophysiology

Tetrodes were fabricated using 12.5-micron nichrome wire (Sandvik-Kanthal) following standard procedures (Siegle et al., 2017; Nguyen et al., 2009; Kloosterman et al., 2009). Tetrodes were threaded through 42 AWG polyimide guide tubes into 8x2 grids of 34 AWG tubes (Small Parts) and glued to a single-screw micro-drive. The drive was modified from a design in Mendoza et al. (2016) and Vandercasteele et al. (2012), in which a 3-pin 0.1'' header served as the skeleton of the drive, with a #0-80 screw replacing the middle pin, and the header's plastic serving as the shuttle. In the experiments reported here, the tetrodes were not advanced after recording sessions started. The tetrodes were plated with a mixture of gold (Neuralynx) and polyethylene glycol (PEG) as per Ferguson et al. (2009), to an impedance of $\sim 100-250K\Omega$. The ground and reference wires were bridged and implanted through a craniotomy above the cerebellum.

Electrode signals were acquired at 30 kHz using custom-made Intan-based 64-channel headstages (Dhawale et al., 2017) and Opal-Kelly FPGAs (XEM6010 with Xilinx Spartan-6 ICs). Spikes were extracted following procedures described in Dhawale et al. (2017). Multiunit firing rates were estimated in non-overlapping 10-ms bins from extracted spikes. Multiunit and single-unit firing rates were Gaussian-filtered and in some cases z-scored. Z-scoring was done using the mean and standard deviation of the response taken over a 2 s window around the peak head velocity after averaging out trials and/or tetrodes. Single-units were sorted using MountainSort (Chung et al., 2017) and classified into putative excitatory regular-spiking units (RSUs) or putative inhibitory fast-spiking units (FSUs) based on the trough-to-peak time (width) and full-width at half-max (FWHM) of the unfiltered waveforms (Figure S2).

Viral Tracing

In order to localize the V1-projecting portion of M2, viral tracing experiments between these two regions were performed using retrograde viruses and with conditional expression of fluorophores (Figure S5). retro-AAV-GFP (Janelia) and retro-AAV-Cre (AAV pmSyn1-EBFP-Cre; Addgene #51507 (Madisen et al., 2015)) were injected into three sites in V1, at 6.35 mm anterior-posterior axis (AP), 4.55 mm mediolateral (ML), 6.0 AP, 4.47 ML, and 5.8 AP, 4.5 ML, at 1 mm below the brain surface, with 500 nL at each site, injected at 25 nl/min using an UMP3 UltraMicroPump (WPI). Into putative V1-projecting portion of M2, FLEX-tdTomato (AAV-CAG-FLEX-tdTomato, UNC Vector core) was injected at two sites (0.5 mm AP, 1.0 mm ML, 1.8 mm DV; −0.5 AP, 0.9 ML, 1.8 and 0.8 DV; 200 nL each at 25nl/min). With this strategy, we were able to visualize retrogradely-labeled inputs to V1 in green and V1-projecting M2 axons in red, imaged on slices stained for GFP (Rabbit Anti-GFP, Life Technologies A11122, 1:1000; Alexa Fluor 488 Goat Anti-Rabbit, Life Technologies A-11034, 1:1000) and for RFP (Chicken Anti-RFP, Sigma, AB3528, 1:500; Alexa Fluor 568 Goat Anti-Chicken IgG, Life Technologies, A-11041, 1:1000) using an Axio Scan.Z1 slide scanner (Zeiss).

Lesions

Lesions of M2 were performed using excitotoxic injections of ibotenic acid (IA) (Abcam ab120041) delivered using an UMP3 UltraMicroPump (WPI) during two separate procedures. Aliquots of IA were prepared at 1% concentration and frozen. In the first procedure, IA was injected into four sites in one hemisphere (1.5 mm AP, relative to Bregma and 1.0 mm ML; 0.5 AP, 0.75 ML; −0.5 AP, 0.75 ML; and −1.5 AP, 0.75 ML, with two injections per site, at 1.6 and 0.8 mm below the brain surface, 75 nL each) and the animal was allowed to recover for one week, after which the injections were repeated at the same sites in the opposite hemisphere and electrode arrays were implanted in V1.

Micro-CT

X-ray micro-computed-tomography (micro-CT) was used to quantify lesion sizes and locations and to determine the depth of implanted electrodes after performing electrolytic lesions through the implanted tetrodes by passing $40\mu A$ through each wire for

Please cite this article in press as: Guitchounts et al., Encoding of 3D Head Orienting Movements in the Primary Visual Cortex, Neuron (2020), https://doi.org/10.1016/j.neuron.2020.07.014

15 s (Masís et al., 2018b). To extract brains, rats were deeply anesthetized with sodium pentobarbital (180 mg/kg; Fatal-Plus C IIN, Vortech Pharmaceuticals, Dearborn, MI) and perfused with paraformaldehyde (#15710, Electron Microscopy Sciences (EMS), Hatfield, PA) and glutaraldehyde (#16220, EMS). Brains were then stained with osmium (VWR 19190) for two weeks and embedded in resin before imaging using a Nikon Metrology X-Tek HMX ST 225 Micro-CT scanner (Nikon Metrology Ltd., Tring, UK). This method, which was previously described in detail in Masis et al. (2018a, 2018b), allows characterization of lesions without slicing the brain. Lesion ROIs from scanned brains were analyzed using FIJI (Schindelin et al., 2012) and ITK-SNAP (Yushkevich et al., 2006).

Head Orienting Movement Extraction

HOMs were extracted from the time derivatives of head direction signals (yaw, roll, and pitch) by finding crossings of a threshold (100 deg/s). Consecutive threshold crossings were peak-aligned. Positive and negative crossings of the threshold in the derivative of yaw signal were termed Left and Right HOMs, respectively; similarly, roll crossings were termed clockwise (CW) and counterclockwise (CCW) HOMs, and pitch crossings were termed Up and Down HOMs.

The timing of the MUA firing rates relative to HOM onset were calculated by subtracting session-averaged HOM deviation times from MUA deviation times. MUA deviation times were defined as the time that the mean firing rate crossed the threshold of the 99% bootstrap CI of the baseline interval (-1000 to -750 ms relative to peak head velocity). HOM deviation times were defined as the time that the mean velocity crossed the threshold of $2 \times STD$ of the baseline interval (-1000 to -750 ms relative to peak head velocity).

Movement Classification

In addition to HOMs, rats were classified as moving or resting (Figure 2) based overall movement, which was calculated as the L2 norm of the linear (translational) components of acceleration. Histograms of the overall movement signal showed a bimodal distribution (Figure 2B). The valley between the two peaks was used as the threshold at which the animals were considered to be immobile (resting) or mobile (moving) (Dhawale et al., 2017).

Head Orienting Movement Direction Decoding

HOM direction was decoded using MUA firing rates (Figures 4A–4D) or single-unit firing rates (Figures 4E–4I) using multinomial logistic regression implemented in the Scikit Learn Python package (Pedregosa et al., 2011). In the MUA decoding, model inputs consisted of z-scored firing rates averaged across tetrodes ($N = 16$) and sessions ($N = 86-107$) in a 0.5 s window centered at peak velocity (Figures 4A–4C) or a 0.1 s sliding window -2 to $+2$ sec around peak velocity (Figure 4D). The models were trained and tested on half (Figures 4A and 4B) or varying fractions (Figure 4C) of the sessions. SUA decoding models were constructed similarly, but with each neuron's firing rate contributing a separate feature to the model. The models were trained either to decode opposing HOM directions (e.g., Left versus Right; CW versus CCW; Up versus Down) (Figure 4E), or six-direction classification (Figures 4F–4I). The latter were trained either on varying numbers of HOM bouts (up to $N = 100$ trials) using all neurons (Figure 4G); or with half ($N = 50$) of the trials used for training and the other half for testing, using varying numbers of neurons (Figures 4H and 4I). All models were trained with $N = 100$ random splits of trials or neurons. Each model was threefold cross-validated to find the optimal regularization parameter C (ranging from $1e-03$ to $1e+03$ and penalty (L1 or L2).

Flash Stimulus Presentation and Analysis

Visual stimuli consisted of 500-ms flashes of white LEDs mounted on the ceiling of the home-cage arena, which was fully dark during the flash off-cycle (400-600 ms, uniform random time).

MUA or SUA responses to flash stimuli were quantified in the 100-ms window following stimulus onset and split into three conditions according to the rat's movement parameters within that window: overall movement, in which total acceleration exceeded the movement threshold defined in Figure 2; orienting, in which the angular velocity of the head crossed the 100 deg/s threshold in either of the three axes; or resting, in which the angular velocity and total acceleration were below their thresholds. Post-stimulus time histograms (PSTHs) were smoothed with a Gaussian filter and z-scored.

Responsive cells were manually selected by examining waveforms and mean PSTHs, following which significant responses were selected by discarding trials with zero variance and performing a shuffle test between mean firing rates in the response window (50-ms between 30 and 80 ms after stimulus onset) and a baseline window (50-ms before stimulus onset). Responses during movement and rest were compared using a Mann-Whitney U test in the response window (Figure 6).

QUANTIFICATION AND STATISTICAL ANALYSIS

All statistical comparisons were done using non-parametric tests (e.g., Mann-Whitney U or Wilcoxon signed-rank test) unless specified otherwise. A significance level of alpha = 0.01 was used throughout, unless otherwise noted. Bonferroni correction was applied where appropriate.